united nations
educational, scientific
and cultural
organization

international atomic
energy agency

the
abdus salam
international centre for theoretical physics

SMR/1270-40

SCHOOL ON SYNCHROTRON RADIATION

6 November – 8 December 2000

Miramare - Trieste, Italy

Supported in part by the Italian Ministry of Foreign Affairs in connection with the SESEME project

Co-sponsors: Sincrotrone Trieste, Società Italiana di Luce di Sincrotrone (SILS) and the Arab Fund for Economic and Social Development

Inelastic X-ray Scattering From Electronic Excitations

Michael Krisch
European Synchrotron Radiation Facility
Grenoble, France

Inelastic X-ray Scattering From Electronic Excitations

Michael Krisch
European Synchrotron Radiation Facility
Grenoble, France

krisch@esrf.fr

The two lectures on inelastic x-ray scattering should allow the audience to get a feeling of what can be done with this technique. The necessary theoretical background is layed out and illustrated by several in order to show to which type of problems inelastic x-ray scattering can be applied. The purpose of this short note is a further illustration of the transparency copies and provision of a literature list (for sure incomplete). Due to the limited time available the two lectures can not give a complete overview covering every aspect. Consequently the selection reflects my personal preference, and to a certain extent my own research interest.

The first lecture provides a general introduction, the theoretical background and some instrumental aspects. The lectures will focus on the aspects of IXS which are closely related to other electron spectroscopies, in particular to x-ray absorption spectroscopy (XAS), thus providing a natural link to the other lectures of the week. Consequently, non-resonant valence electron excitations and Compton scattering will not be discussed. First, non-resonant IXS from core electron excitations, as well called x-ray Raman scattering (XRS), will be discussed. In this case, the relation to XAS is very close. As a matter of fact, under certain conditions XRS and XAS yield the same result. XRS allows to perform soft x-ray absorption studies in the hard x-ray regime. This has advantages in the study of systems which are not compatible with an ultra-high vacuum environment, necessary in the soft x-ray regime. Moreover, by varying the momentum transfer Q, the electric dipole selection rule, defining the final state symmetry which can be reached in an absorption process, is relaxed and, for example, electric monopolar transitions become possible.

The second lecture will be devoted to resonant IXS (RIXS) (often called as well resonant Raman scattering (RRS)), where the incident energy is tuned to an absorption edge of the element under study, and the core-hole, created in the absorption process, is filled by an electron from a shallower core level or the filled part of the valence band under emission of an x-ray. For excitation energies above the absorption edge the process is the well known x-ray fluorescence. Examples will illustrate the capability of the technique to identify absorption channels which can not be separated by XAS. Furthermore, polarization dependent RIXS and its application to magnetic materials will be discussed.

LITERATURE LIST

General Introduction

- W. Schülke, Handbook on Synchrotron Radiation, Vol.3, chapter 15, ed. G. Brown and D.E. Moncton, Elsevier (1991). " Inelastic Scattering by electronic excitations."

- Raman emission by x-ray scattering, ed. D.L. Ederer and J.H. McGuire, World Scientific (1996).

Non-resonant inelastic scattering

Valence electron excitations

- W. Schülke et al.; Phys. Rev. B 33, 6744 (1986)." Dynamic structure factor of electrons in Li metal: Inelastic synchrotron x-ray scattering results and interpretationbeyond the random-phase approximation."

- K. Sturm et al.; Phys. Rev. Lett. 68, 228 (1992). " Plasmon-Fano resonance insidethe particle-hole excitation spectrum of simple metals ans semiconductors."

- W. Schülke et al.; Phys. Rev. B 47, 12426 (1993). "Dynamic structure factor of electrons in Al metal studied by inelastic x-ray scattering."

- N. Schell et al.; Phys. Rev. Lett. 74, 2535 (1995). "Electronic excitations in hcp 4He at 61.5 MPa and 4.3 K studied by inelastic x-ray scattering spectroscopy."

X-ray Raman scattering

- Y. Mizuno et al.; J. Phys. Soc. Jpn. 22, 445 (1967). "Theory of x-ray Raman scattering"

- W. Schülke et al.; Phys. Rev. B 38, 2112 (1988). "Interband transitions and core excitation in highly oriented pyrolythic graphite studied by inelastic synchrotron x-ray scattering: Band structure information."

- H. Nagasawa et al.; J. Phys. Soc. Jpn. 58, 710, (1989). "X-ray Raman spectrum of Li, Be and graphite in a high-resolution inelastic synchrotron x-ray scattering experiment."

- M.H. Krisch et al.; Phys. Rev. Lett. 78, 2843 (1997)." Momentum transfer dependence of inelastic x-ray scattering from the Li K-edge."

D.T. Bowron et al.; Phys. Rev. B 62, R9223 (2000). " X-ray Raman scattering from the oxygen K edge in liquid and solid water."

Resonant x-ray inelastic scattering

Theory, General

- T. Aberg et al.; in atomic inner-shell physics, ed. B. Crasemann, chapter 10, Plenum press (1980). "Inelastic x-ray scattering including resonance phenomena"

- P. Carra et al.; Phys. Rev. Lett. 74, 3700 (1995). " High resolution x-ray resonant Raman scattering."

RRS, various aspects

- P. Eisenberger et al.; Phys. Rev. B 13, 2377 (1976)." Resonant x-ray Raman scattering studies using synchrotron radiation."

- K. Hämäläinen et al.; J. Phys. Condens. Matter 1, 5955 (1989). " Resonant Raman scattering and inner-shell hole widths in Cu, Zn and Ho."

- F.M.F. de Groot et al.; J. Phys. Condens. Matter 6, 6875 (1994). "Charge transfer multiplet calculations of the Kb x-ray emission spectra of divalent nickel compounds".

- M.H. Krisch et al.; Phys. Rev. Lett. 74, 4931 (1995). " Evidence for a quadrupolar excitation channel at the LIII edge of gadoliniumby resonant inelastic x-ray scattering."

- F.M.F. de Groot; Phys. Rev. B 53, 7099 (1996). " 3s2p inelastic x-ray scattering of CaF2."

- M. van Veenendaal et al.; Phys. Rev. B 54, 16010 (1996). " X-ray resonant Raman scattering in the rare earths."

- M. Nakazawa et al.; J. Phys. Soc. Jpn. 65, 2303 (1996). " Theory of resonant x-ray emission spectra in Ce compounds."

- J.P. Rueff et al.; Phys. Rev. Lett. 82, 3284 (1999).

- J.P. Rueff et al.; Phys. Rev. B 60, 14510 (1999). "Magnetic and structural α–ε phase transition in Fe monitored by x-ray emission spectroscopy."

Polarization dependent x-ray emission

- C.F. Hague et al.; Phys. Rev. B 48, 3560 (1993). "Observation of magnetic circular dichroism in Fe L2,3 x-ray fluorescence spectra."

- L.-C. Duda et al.; Phys. Rev. B 50, 16758 (1994). "Magnetic dichroism in L2,3 emission of Fe, Co and Ni following energy-dependent excitation with circularly polarized x-rays."

- M.H. Krisch et al.; Phys. Rev. B 54, R12673, (1996)." Observation of magnetic circular dichroism in the resonant inelastic x-ray scattering at the L3 edge of gadolinium metal."

- F.M.F. de Groot et al.; Phys. Rev. B 56, 7285, (1997). " A Theoretical Analysis of the Magnetic Circular Dichroism in the 2p3d and 2p4d X-ray Emission of Gd."

- F.M.F. de Groot et al.; Phys. Rev. B 62, 379, (2000). " Magnetic linear dichroism in x-ray emission spectroscopy: Yb in $Yb_3Fe_5O_{12}$."

Band structure mapping

- M. van Veenendaal et al.; Phys. Rev. Lett. 78, 2839 (1997). " Excitons and resonant inelastic x-ray scattering in graphite."

- Y. Ma et al.; Phys. Rev. Lett. 69 2598 (1992). " Soft x-ray resonant inelastic scattering at the C K edge of diamond."

- P.D. Johnson et al.; Phys. Rev. B 49, 5024 (1994)." Band structure and x-ray resonant inelastic scattering."

- A. Kaprolat et al.; Appl. Phys. A 65, 169 (1997). "Resonant fluorescenceemission from the Ge and Cu valence band."

Low energy excitations

- S.M. Butorin et al.; Phys. Rev. Lett. 77, 574 (1996). "Resonant x-ray fluorescence spectroscopy of correlated systems: A probe of charge-transfer excitations."

- S.M. Butorin et al.; Phys. Rev. B 54, 4405 (1996). " Low-energy d-d excitations in MnO studied by resonant x-ray fluorescence spectroscopy."

- C.C. Kao et al.; Phys. Rev. B 54, 16361 (1996). "X-ray resonant Raman scattering in NiO: Resonant enhancement of the charge-transfer excitations."

- J.-J. Gallet et al.; Phys. Rev. B 54, 14238 (1996). "4d resonant inelastic x-ray scattering in gadolinium."

Inelastic X-ray scattering from electronic excitations

Michael Krisch
European Synchrotron Radiation Facility
Grenoble, France

krisch@esrf.fr

Introduction
Theoretical Background
Experimental aspects

X-ray Raman scattering
Resonant inelastic x-ray scattering

The Scattering Kinematics

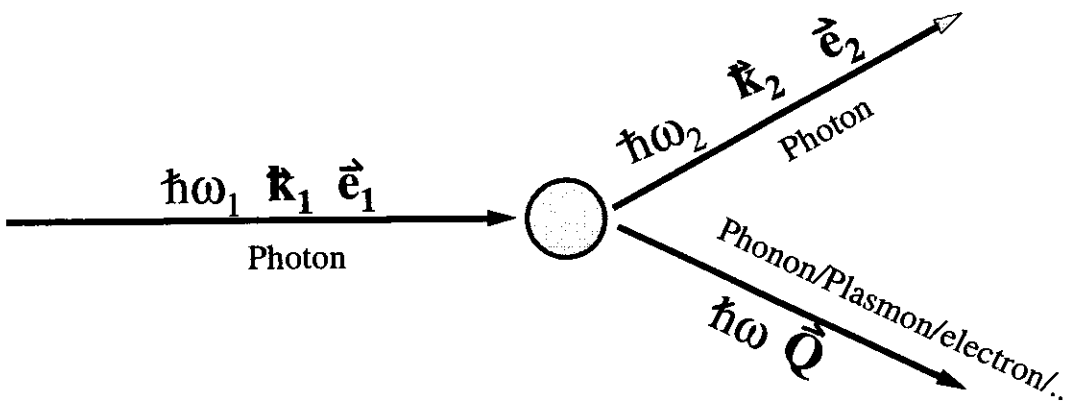

$\vec{Q} = \vec{k}_1 - \vec{k}_2$	Momentum transfer
$\hbar\omega = \hbar\omega_1 - \hbar\omega_2$	Energy transfer

Schematic inelastic x-ray spectrum

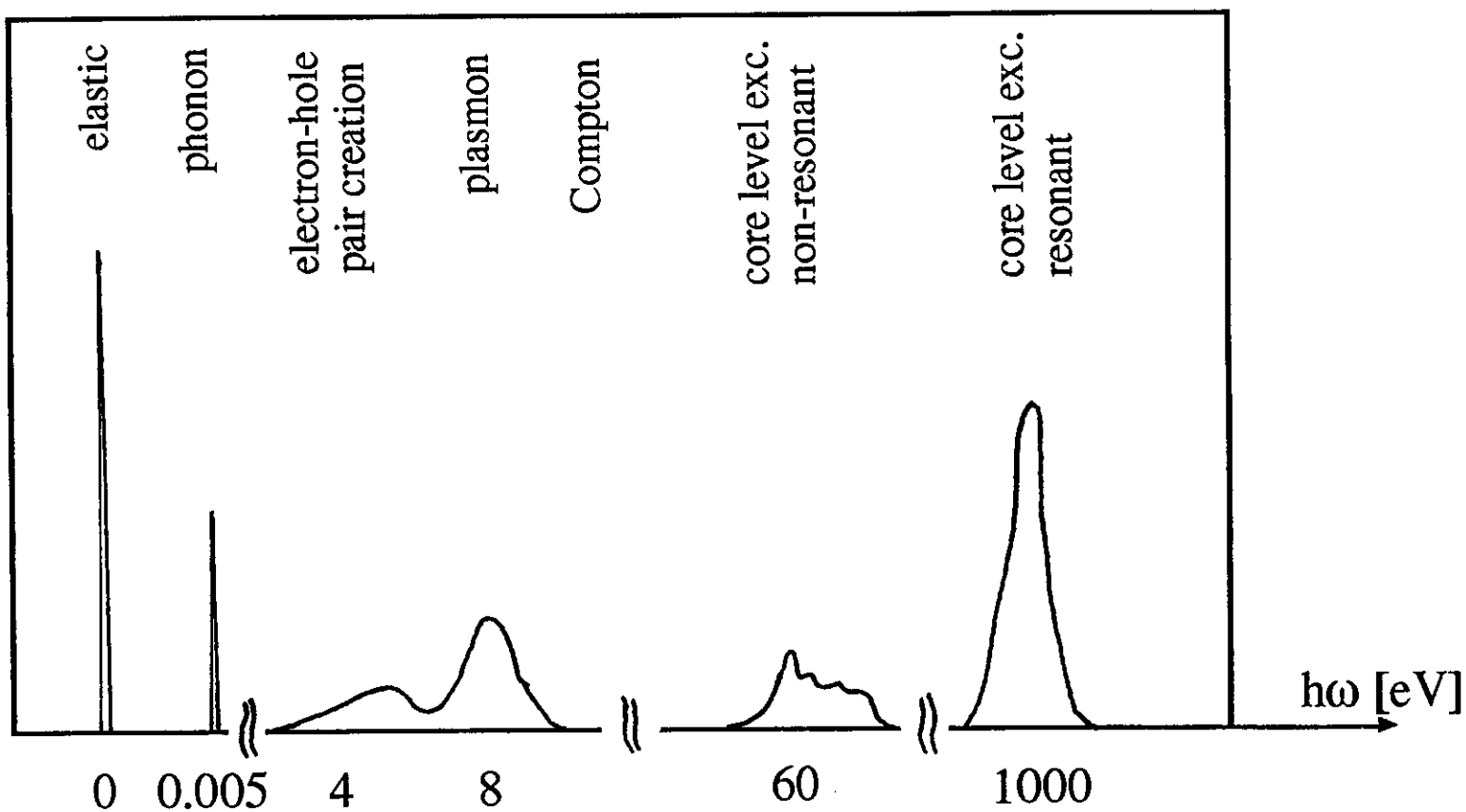

Theoretical Background

Electron-photon interaction Hamiltonian (non-relativistic):

$$H_{\text{int}} = \frac{e}{m_e c} \sum_j \left(\frac{e}{2c} \vec{\mathbf{A}}_{\mathbf{j}}^{\mathbf{2}} + \vec{\mathbf{A}}_{\mathbf{j}} \vec{\mathbf{p}}_{\mathbf{j}} \right)$$

j is the summation over the electrons of the scattering system.

Vector potential of the electromagnetic field:

$$\vec{\mathbf{A}}_j = \sqrt{\frac{4\pi c^2}{V}} \sum_{\vec{\mathbf{k}},q} \left(\vec{\mathbf{e}}_{\vec{\mathbf{k}},q} a_{\vec{\mathbf{k}},q} e^{i\vec{\mathbf{k}}\vec{\mathbf{r}}_j} + \vec{\mathbf{e}}^{*}_{\vec{\mathbf{k}},q} a^{+}_{\vec{\mathbf{k}},q} e^{-i\vec{\mathbf{k}}\vec{\mathbf{r}}_j} \right)$$

$\vec{\mathbf{e}}_{\mathbf{k},\mathbf{q}}$ and $\vec{\mathbf{k}}$ are the polarization vector and the wave vector of the photon field component with frequency ν and $n_{\mathbf{k}}$ photons in the mode. The index q (=1,2) labels the two polarizations of each plane wave with wave vector $\vec{\mathbf{k}}$.

Photon creation- and annihilation operator:

$$a^{+}_{n_{k+1},n_k} = a_{n_k,n_{k+1}} = \sqrt{\hbar(n_k+1)/2\nu_k}$$

Momentum operator of the electron:

$$\vec{\mathbf{p}} = -i\hbar\vec{\nabla}$$

Lowest order perturbation theory (Fermi's Golden Rule):

$$w_{i\to f} = \frac{2\pi}{\hbar}\left|\underbrace{\langle F|H_{\text{int}}|I\rangle}_{\text{1. order}} + \underbrace{\sum_N \frac{\langle F|H_{\text{int}}|N\rangle\langle N|H_{\text{int}}|I\rangle}{E_N - E_I}}_{\text{2. order}}\right|^2 \delta(E_F - E_I - \hbar\omega)$$

1) $\mathbf{p}\cdot\mathbf{A}$ in 1. Order: absorption or emission of a photon

2) $\mathbf{A}^2$ in 1. Order: non-resonant inelastic x-ray scattering

3) $\mathbf{p}\cdot\mathbf{A}$ in 2. Order: resonant inelastic x-ray scattering

Double differential cross section

$$\frac{d^2\sigma}{d\omega_2 d\Omega} = \sum_F w_{i\to f}\ \rho(E_f) I_0^{-1}$$

$w_{i\to f}$ is the transition probability, $\rho(E_f)$ is the density of final states and I_0 the incident flux.

$$\frac{d^2\sigma}{d\omega_2 d\Omega} = r_0^2 \frac{\omega_2}{\omega_1} \sum_{I,F} \left| \langle F | \sum_j e^{i(\vec{\mathbf{k}}_1 - \vec{\mathbf{k}}_2)\vec{\mathbf{r}}_j} | I \rangle (\vec{\mathbf{e}}_1 \cdot \vec{\mathbf{e}}_2) \right. \qquad \text{(non-resonant part)}$$

$$\left. + \frac{1}{m_e} \sum_N \frac{\langle F | \vec{\mathbf{e}}_2 \sum_j \vec{\mathbf{p}}_j e^{-i\vec{\mathbf{k}}_2\vec{\mathbf{r}}_j} | N \rangle \langle N | \vec{\mathbf{e}}_1 \sum_j \vec{\mathbf{p}}_j e^{i\vec{\mathbf{k}}_1\vec{\mathbf{r}}_j} | I \rangle}{E_I - E_N + \hbar\omega_1 + 0.5i\Gamma_N} \right|^2 \qquad \text{(resonant part)}$$

$$\delta(E_F - E_I - \hbar\omega) \qquad \text{(energy conservation)}$$

Experimental Setup (ID16 at ESRF)

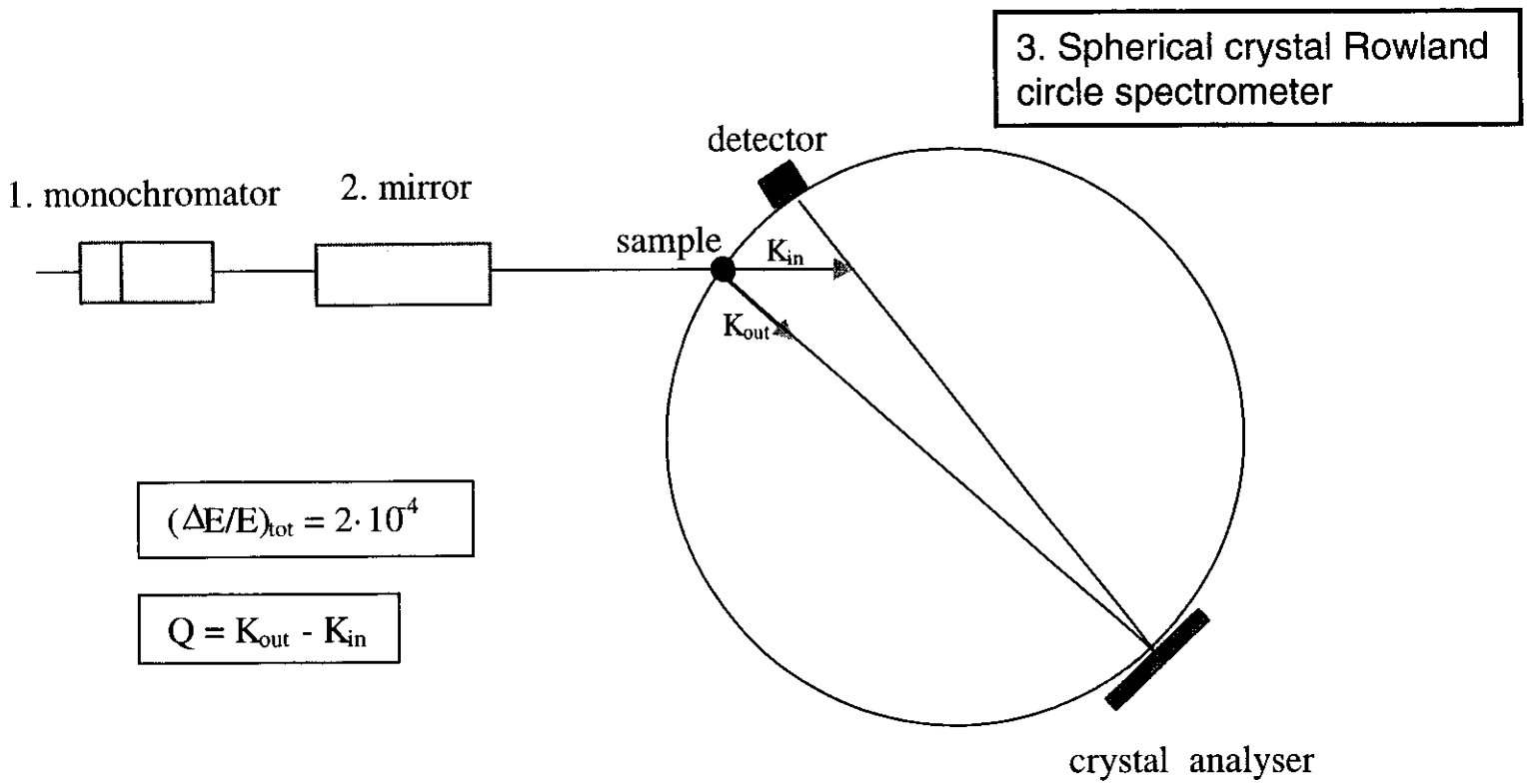

1. Si (111) scanning double crystal monochromator.
2. Toroidal mirror to produce small focal spot at sample.
3. Crystal spectrometer to energy analyze the scattered photons:
   1m spherical crystal, typically Si (440) to Si (555) at Bragg angles 65° - 90°.

Scanning modes

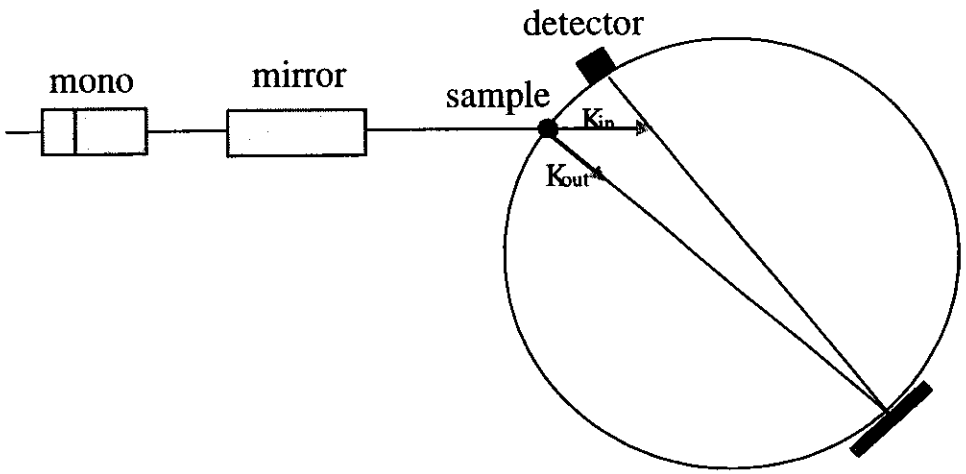

1. $\hbar\omega_2$ fixed, scanning $\hbar\omega_1$ — non-resonant IXS

2. $\hbar\omega_1$ fixed, scanning $\hbar\omega_2$ — RIXS
   (rotating crystal and follow with the detector)
3. Scanning $\hbar\omega_1$ and $\hbar\omega_2$ — RIXS
   (keeping energy transfer constant)

X-ray Raman scattering

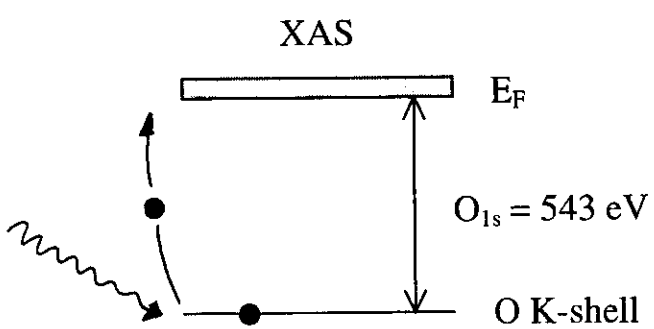

$E_{1s} + e_k = h\omega_1$

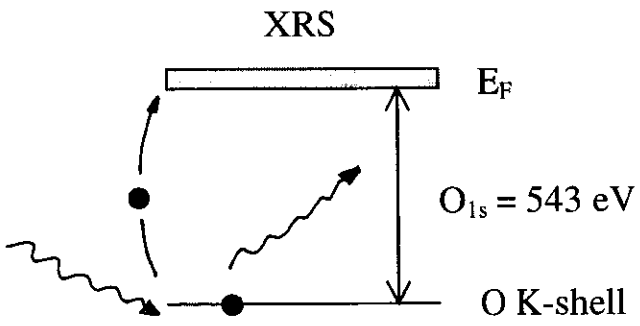

$E_{1s} + e_k = h\omega = h\omega_1 - h\omega_1$

The role of the incident photon energy in XAS is played by the energy transfer in XRS

=>

certain freedom in the choice of the incident photon energy

$$\frac{d^2\sigma}{d\omega_2 d\Omega} = r_0^2 \frac{\omega_2}{\omega_1} (\vec{\mathbf{e}}_1 \cdot \vec{\mathbf{e}}_2) \sum_F \left| \langle F | \sum_j e^{i\vec{\mathbf{Q}}\vec{\mathbf{r}}_j} | I \rangle \right|^2 \delta(E_F - E_I - \hbar\omega)$$

X-ray absorption cross section (dipolar approximation):

$$\frac{d\sigma}{d\omega_1} = 4\pi^2 \alpha \hbar \omega_1 \sum_F \left| \langle F | \vec{\mathbf{e}}_1 \cdot \vec{\mathbf{r}} | I \rangle \right|^2 \delta(E_F - E_I - \hbar\omega_1)$$

X-ray Raman cross section:

$$\frac{d^2\sigma}{d\omega_2 d\Omega} = r_0^2 \frac{\omega_2}{\omega_1} (\vec{\mathbf{e}}_1 \cdot \vec{\mathbf{e}}_2) \sum_F \left| \langle F | \sum_j e^{i\vec{\mathbf{Q}}\vec{\mathbf{r}}_j} | I \rangle \right|^2 \delta(E_F - E_I - \hbar\omega)$$

$Qr \ll 1$: $e^{iQr} \approx 1 + iQr$

Dipolar regime: identical to photon absorption, where **Q** plays the role of the photon polarization vector $\mathbf{e}_1$.

$Qr > 1$: e^{iQr}

Multipolar regime: monopolar, dipolar and quadrupolar transitions possible.

X-ray Raman scattering from the O K-edge in water and ice

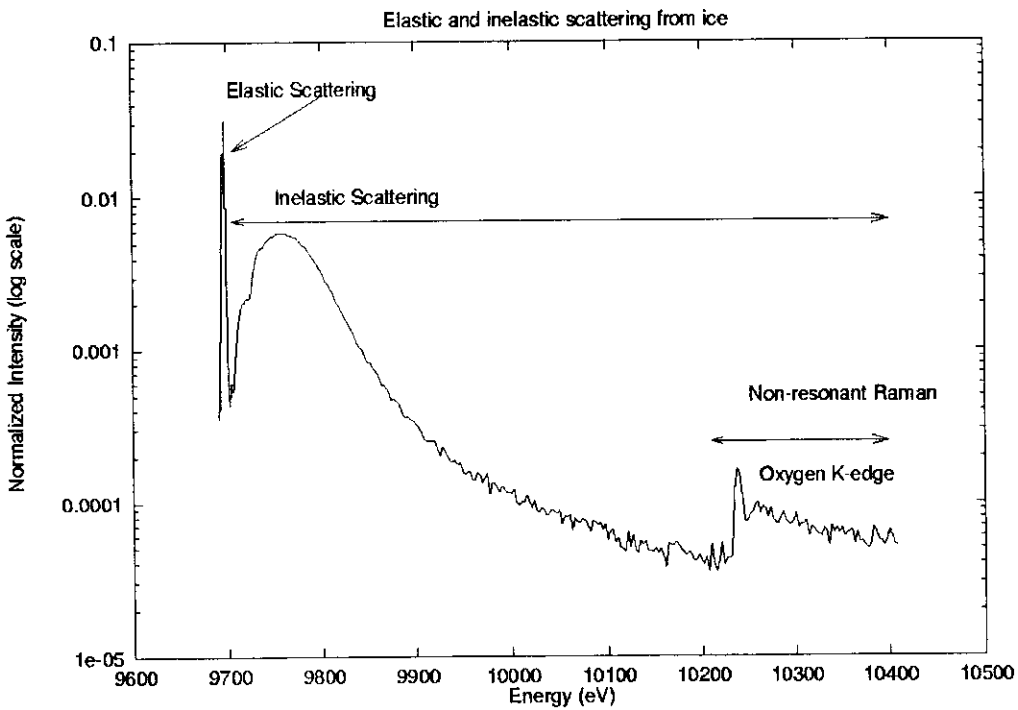

$\hbar\omega_2 = 9686$ eV

$\Delta E = 2$ eV

$Q = 4.38$ A^{-1} ($Qr = 0.29$)

$k < 7$ A^{-1}

Comparison of Oxygen K-edge spectrum in water and Ice Ih

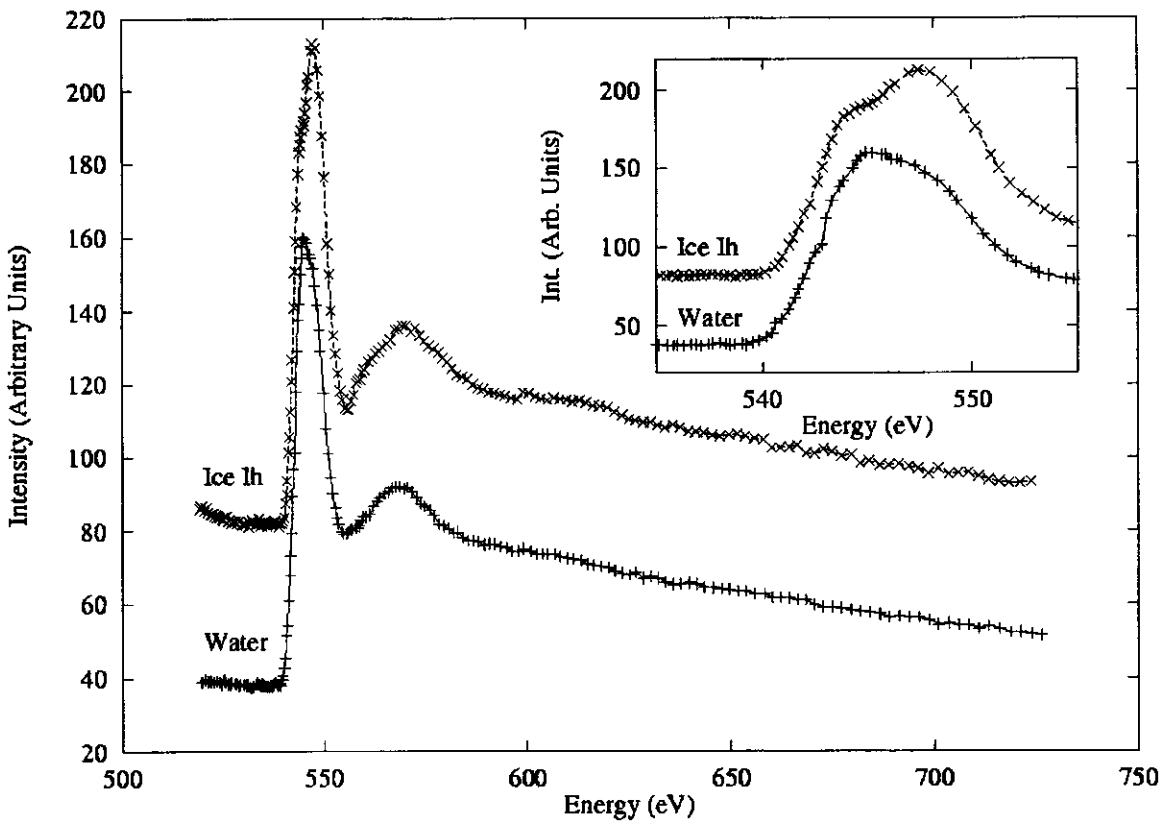

EXAFS Analysis

1) Analysis of Ice Ih IRS data using known structure of Ice Ih.
2) Extraction of parameters that govern the distance scale and the coordination number.
3) Transfer of the parameters to the liquid state analysis.
4) Refinement of the liquid state IRS data.

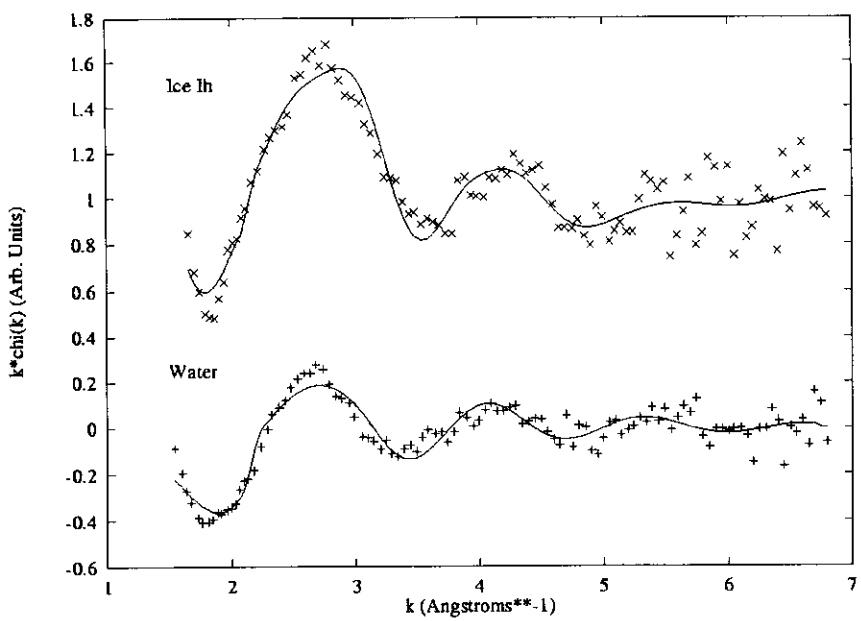

O-O partial radial distribution function

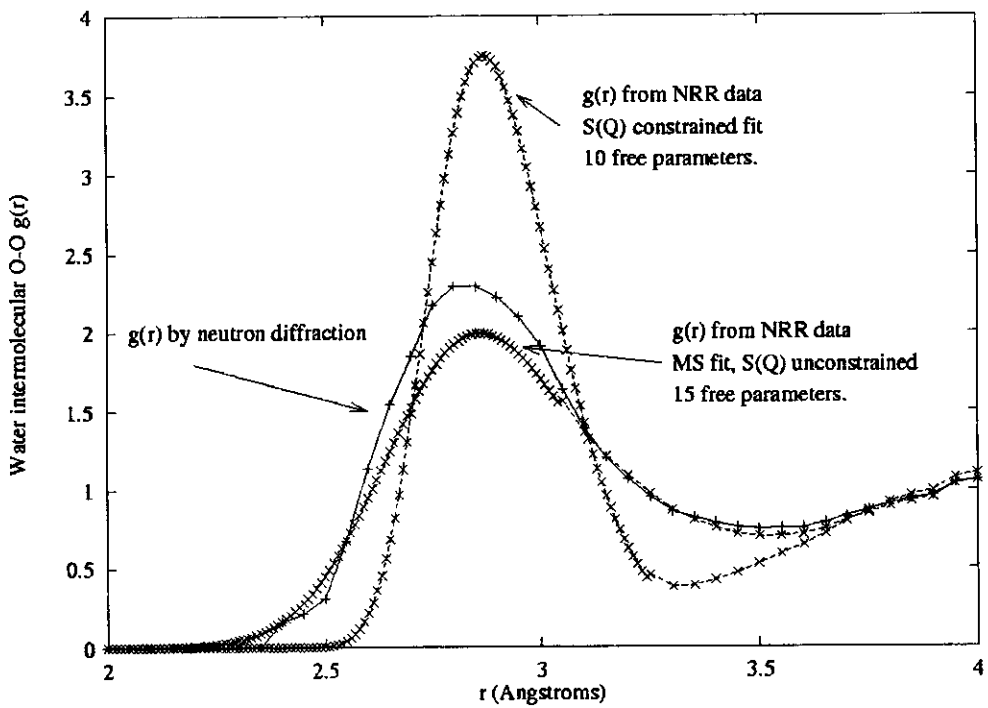

X-ray Raman Scattering:
O-O distance: 2.87 Å
Coordination: 4 - 7

Neutron Scattering:
O-O distance: 2.85 Å
Coordination: 4.4

Probing final states beyond the dipole selection rules

Lithium metal, E_{inc} = 10 keV, ΔE = 80 meV

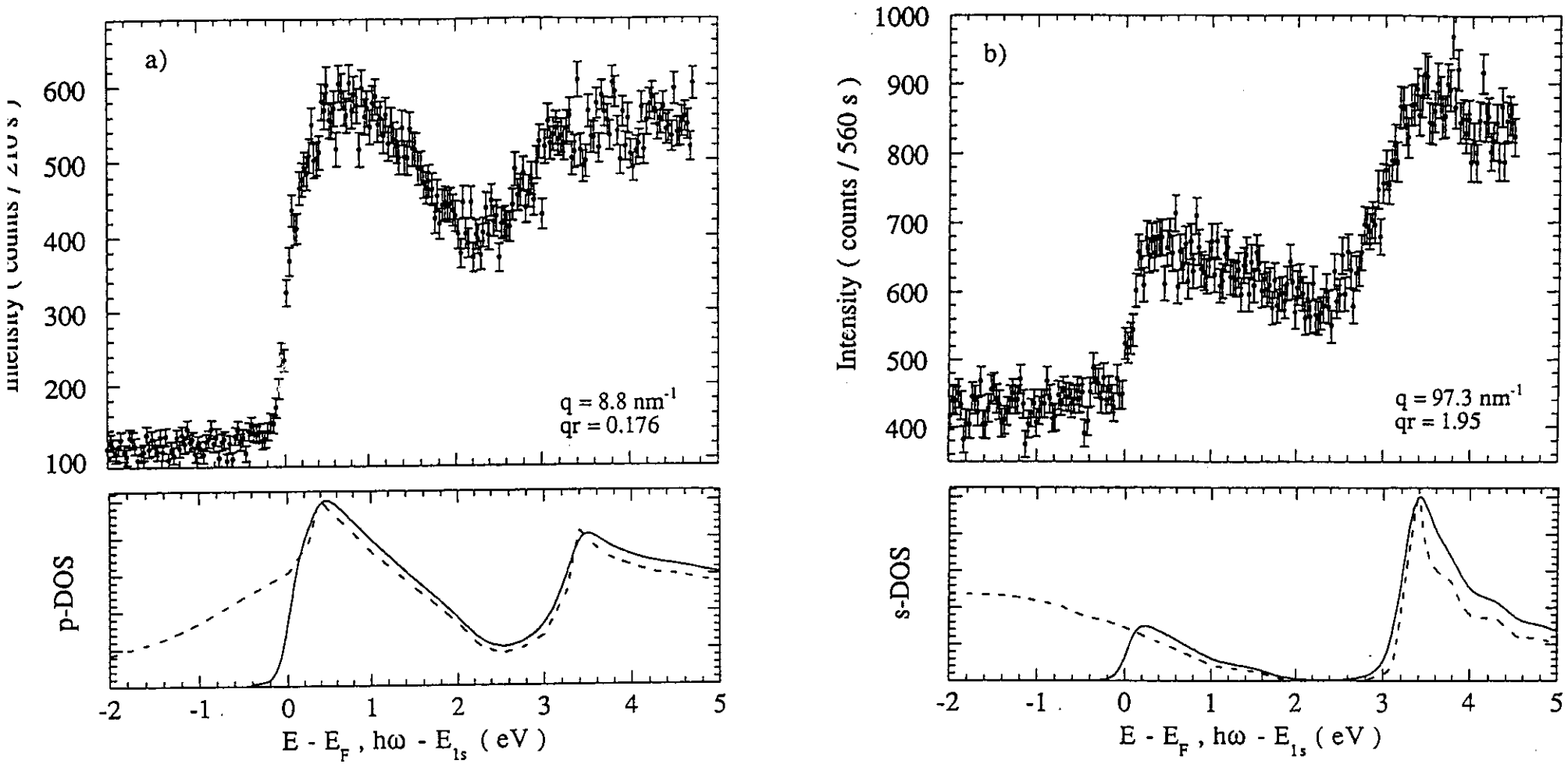

Summary

Soft x-ray spectroscopy in the hard x-ray regime

- "simple" sample environment
- bulk sensitive
- access "exotic" final states
- extreme conditions: high temperature, high pressure

Weak probe

- practically limited to $Z < 14$
- limited quality for structural analysis (EXAFS)
- reasonable quality in the XANES region
- for high T, P measurements: cell window contribution critical

Exploit information contained in the near-edge region.

Resonant inelastic x-ray scattering

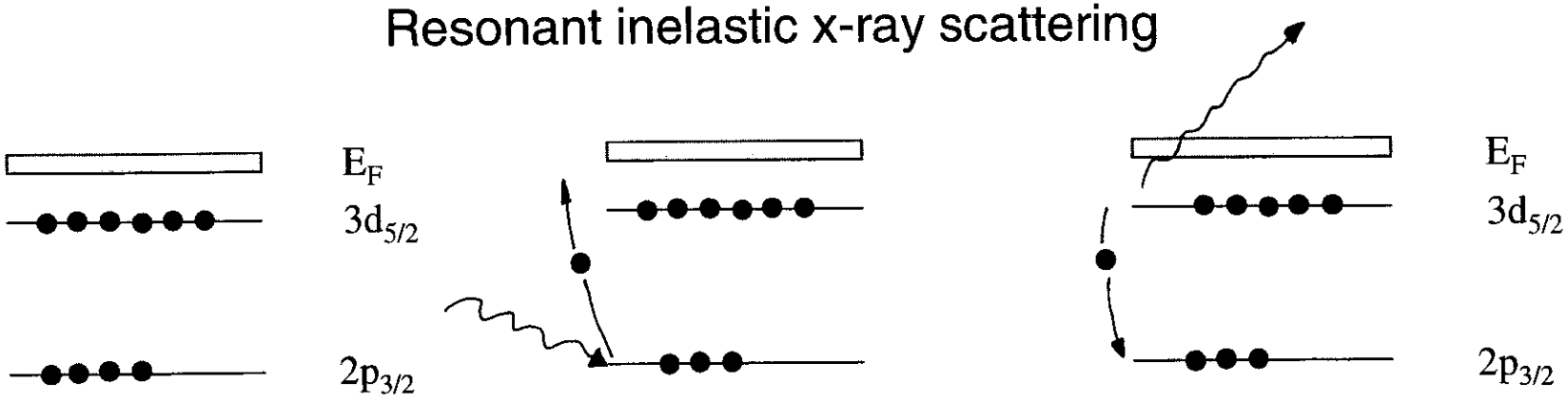

$E_{2p} + e_k = \hbar\omega_1$

$E_{3d} + e_k = \hbar\omega = \hbar\omega_1 - \hbar\omega_2$

$$\frac{d^2\sigma}{d\omega_2 d\Omega} = r_0^2 \frac{\omega_2}{\omega_1} \sum_{I,F} \left| \frac{1}{m_e} \sum_N \frac{\langle F | \vec{\mathbf{e}}_2 \sum_j \vec{\mathbf{p}}_j e^{-i\vec{\mathbf{k}}_2 \vec{\mathbf{r}}_j} | N \rangle \langle N | \vec{\mathbf{e}}_1 \sum_j \vec{\mathbf{p}}_j e^{i\vec{\mathbf{k}}_1 \vec{\mathbf{r}}_j} | I \rangle}{E_I - E_N + \hbar\omega_1 + 0.5i\Gamma_N} \right|^2 \delta(E_F - E_I - \hbar\omega)$$

The RIXS cross section in a more compact way

$$\frac{d^2\sigma}{d\omega_2 d\Omega} \approx \sum_{q'=0,\pm1} \sum_{q=0,\pm1} F_{q,q'}\, \delta(E_F - E_I - \hbar\omega)$$

$$F_{q,q'} = \sum_F \left| \sum_N \frac{\langle F | C_{q'}^{(m')} | N \rangle \langle N | C_q^{(m)} | I \rangle}{E_I - E_N + \hbar\omega_1 + 0.5i\Gamma_n} \right|^2$$

- q and q' denote the polarization states of the incident and scattered photon:
  - q = 0: linear polarized x-rays parallel to the quantization axis.
  - q = 1: right circular polarized x-rays perpendicular to the quantization axis.
  - q = -1: left circular polarized x-rays perpendicular to the quantization axis.

- $C^{(m)}$ and $C^{(m')}$ are the transition operators of the excitation and deexcitation step, expressed in spherical harmonics:
  m=1, electric dipole (E1); m=2, electric quadrupole (E2)

Some characteristics of the RIXS cross section

- Energy resolution of RIXS spectra limited by final state hole lifetime.
- Resonance condition, if $\hbar\omega_1 = E_N - E_I$.

Below threshold: $\hbar\omega_1 < E_N - E_I$

$\hbar\omega_2 - \hbar\omega_1 = E_{3d}$

$\hbar\omega_{2,max} = \hbar\omega_1 - E_{3d}$ Raman dispersion

Above threshold:

(i) excitation into continuum states:

$\hbar\omega_2 - \hbar\omega_1 = E_{3d} + e_k$

$\hbar\omega_1 = E_{2p} + e_k$

$\hbar\omega_2 = E_{2p} - E_{3d}$

(ii) excitation into discrete states with binding energy E* just below the onset of the continuum:

$\hbar\omega_2 - \hbar\omega_1 = E_{3d} - E^*$

$\hbar\omega_2 = E_{2p} - E_{3d}$

Resonant inelastic x-ray scattering at the L-edges of rare-earth materials

Erbium L_3 x-ray absorption of Er_2O_3

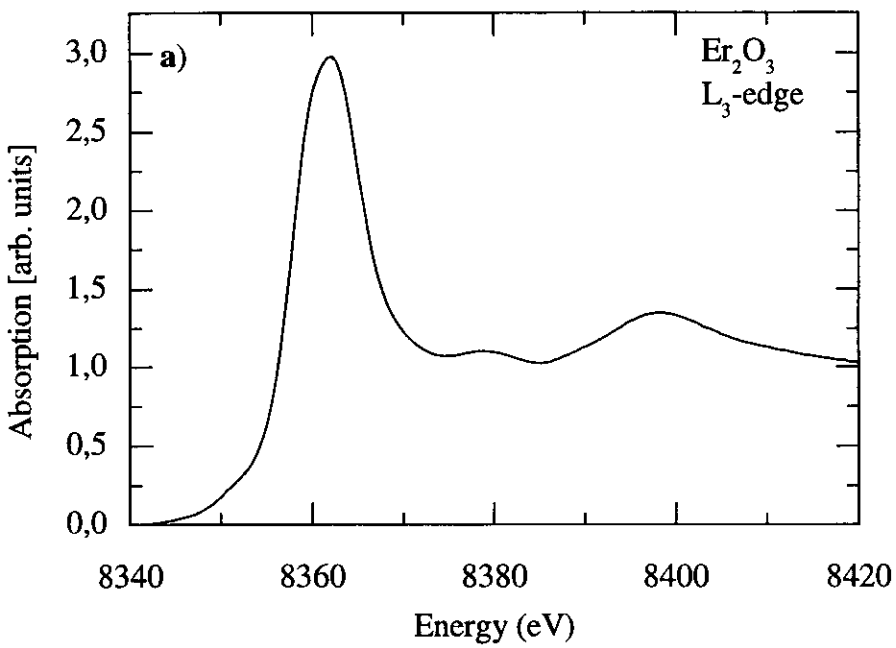

- Energy resolution is limited by the final state core-hole life time.
- Γ_L = 3 - 7 eV for the Rare-Earth elements.

  => additional absorption channels (if existing) might be obscured.

RIXS spectra at fixed incident energies around the absorption edge, monitoring the radiative $3d_{5/2}$ -> $2p_{3/2}$ decay channel.

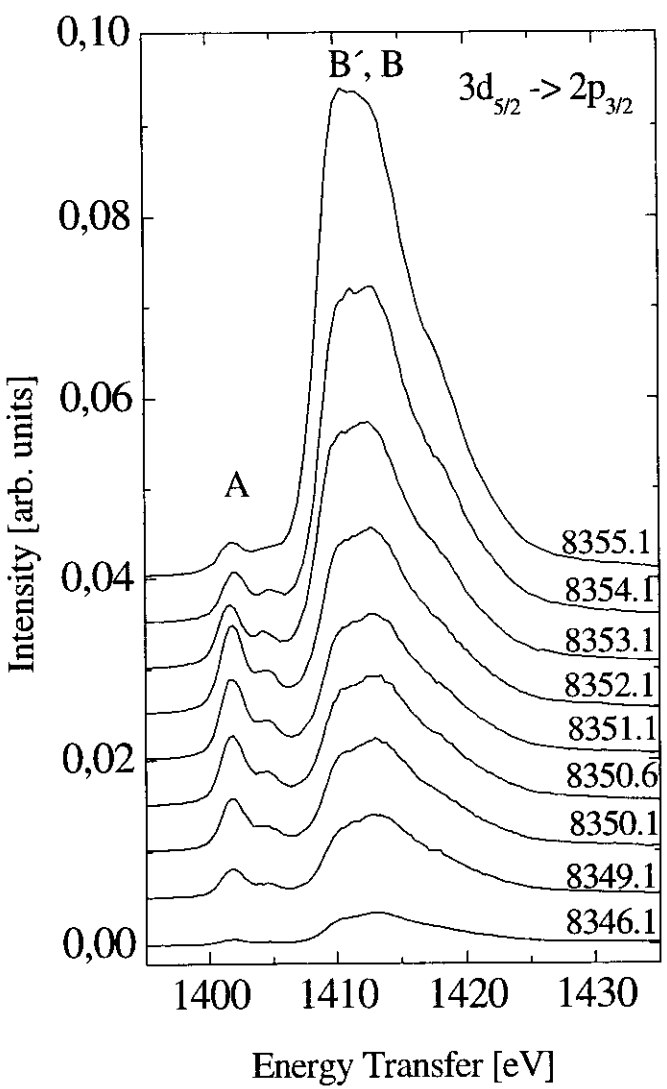

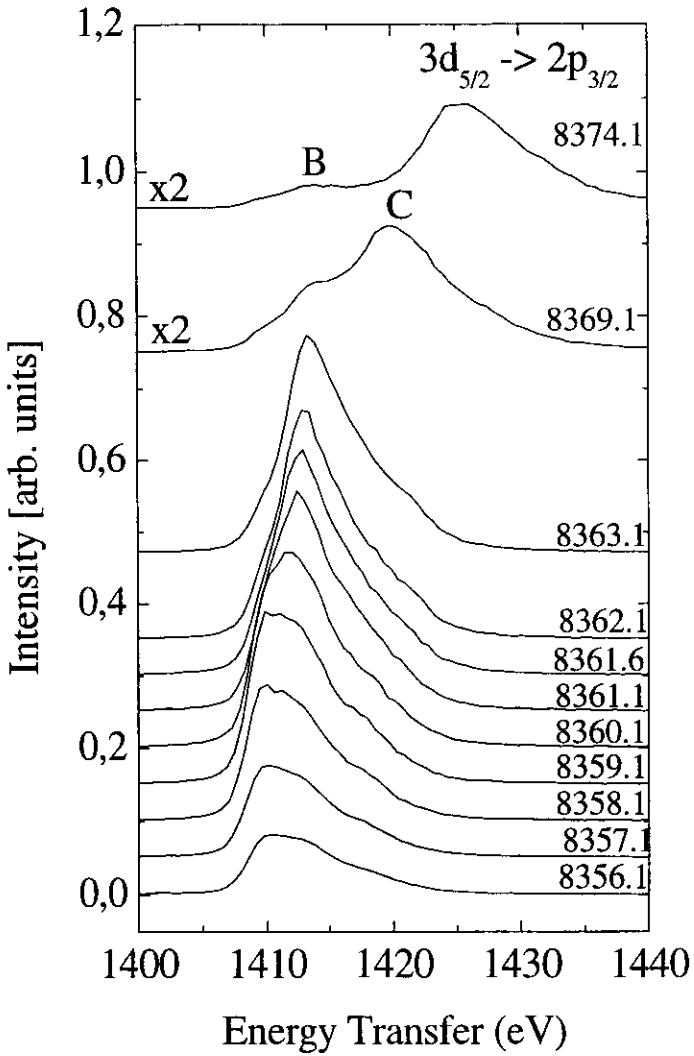

Observation of three different final state multiplet families:

A: very weak, only visible in the pre-edge region, always observed at constant energy transfer.
B: strong, always observed at constant energy transfer.
C: cannot be separated in pre-edge region, above edge observed at increasing energy transfer

Ground state of Er^{3+}: $|I\rangle = |4f^{11}5d^{0}\rangle$

$|F\rangle_c$: $|3d^{9}4f^{11}5d^{0}e_k\rangle$ <= $|N\rangle_c$: $|2p^{5}4f^{11}5d^{0}e_k\rangle$
(E1 excitation into continuum states and observation of $L\alpha_1$ fluorescence)

$|F\rangle_B$: $|3d^{9}4f^{11}5d^{1}\rangle$ <= $|N\rangle_B$: $|2p^{5}4f^{11}5d^{1}\rangle$
(E1 excitation into empty 5d states)

$|F\rangle_A$: $|3d^{9}4f^{12}5d^{0}\rangle$ <= $|N\rangle_A$: $|2p^{5}4f^{12}5d^{0}\rangle$
(E2 excitation into empty 4f states)

Intensity evolution of multiplet families as a function of $\hbar\omega_1$ and character of features within one multiplet family

=>

Constant final state scans: $E_F - E_I = \hbar\omega_2 - \hbar\omega_1 = \text{constant}$

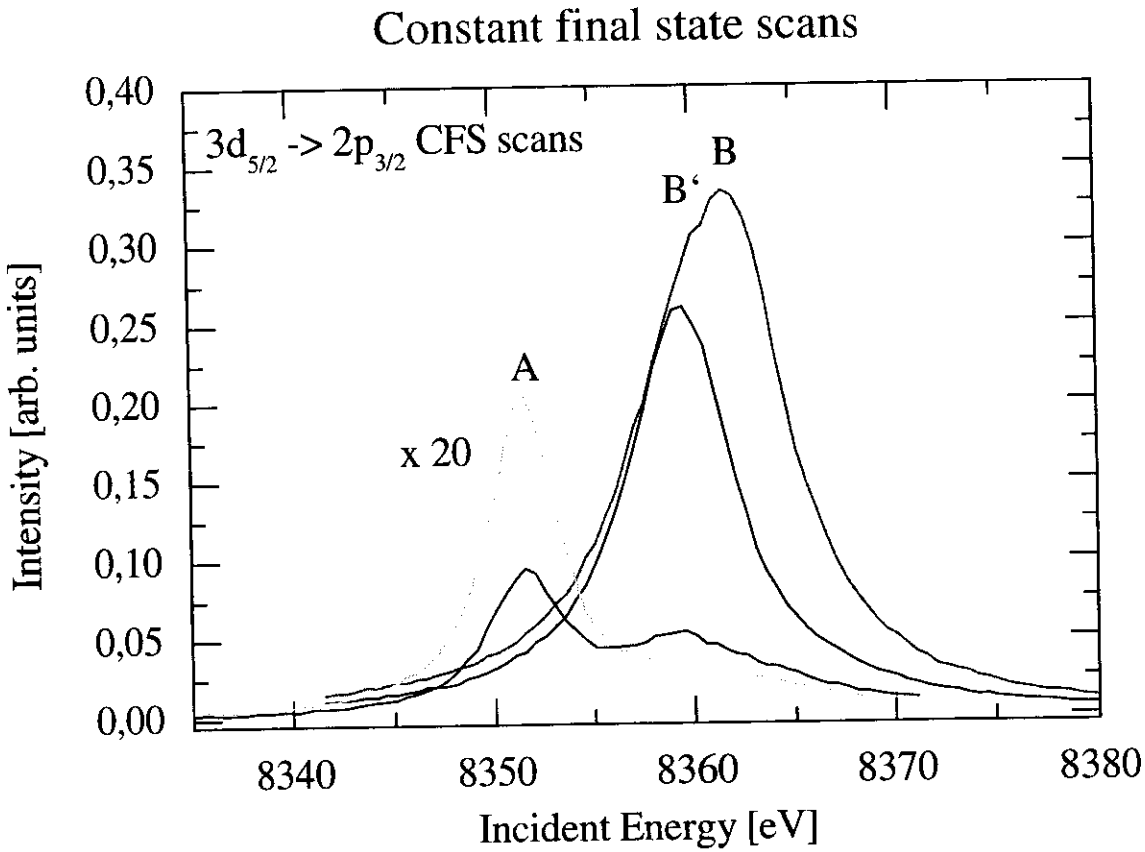

B and B*:
different intermediate states, cubic field splitting of the 5d states: $\Delta E = 2.3$ eV

A and A*: Same intermediate state, splitting due to spread of final state multiplet.

Conclusions

RIXS allows the separation of different excitation channels which are obscured in a standard absorption measurement.

Condition:

Final state core-hole lifetime < energy separation of the multiplet families

Identification of features in the XMCD spectra of magnetic rare-earth materials

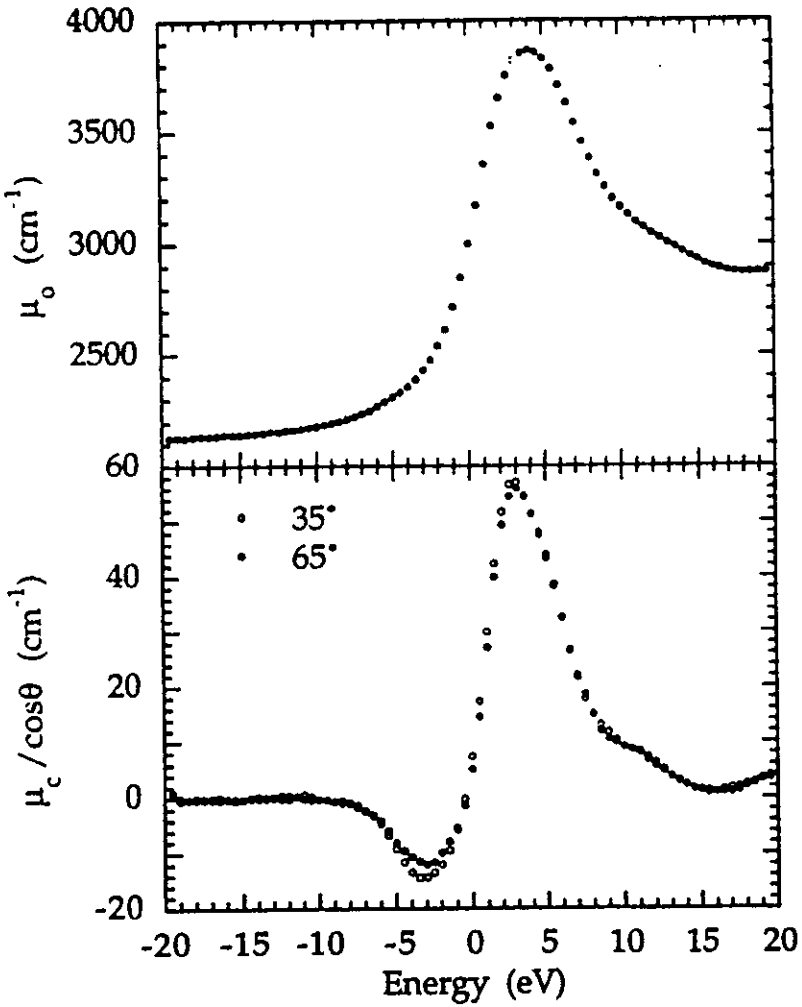

FIG. 1. Dy L_{III} absorption edge (top) and CMXD spectra showing data at 35° and 65° (bottom).

Features in the XMCD spectra do not have a counterpart in the absorption spectrum.

RIXS to reveal additional absorption channels.

Comparison XMCD - RIXS Constant Final State Spectra for $RE_2Fe_{14}B$ compounds

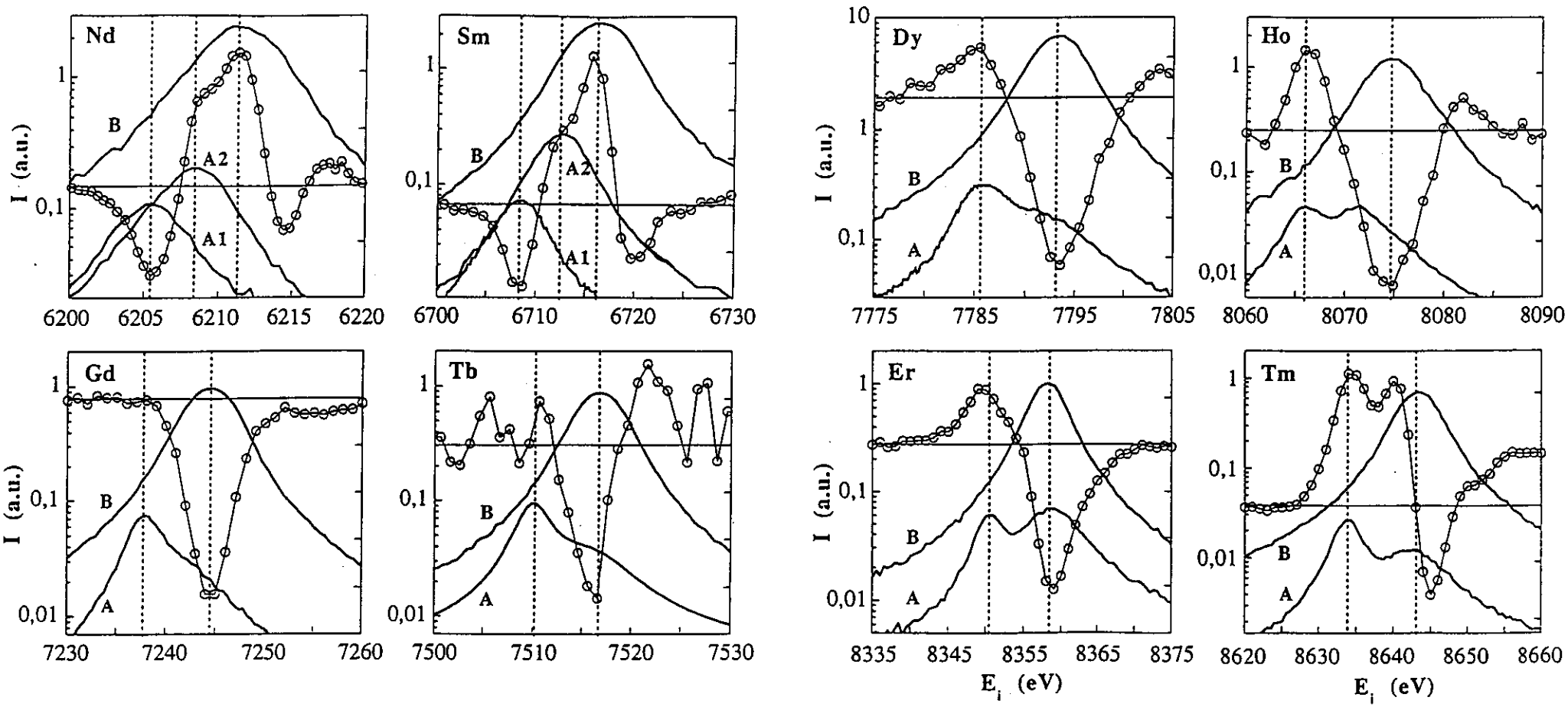

Graphical summary of the results

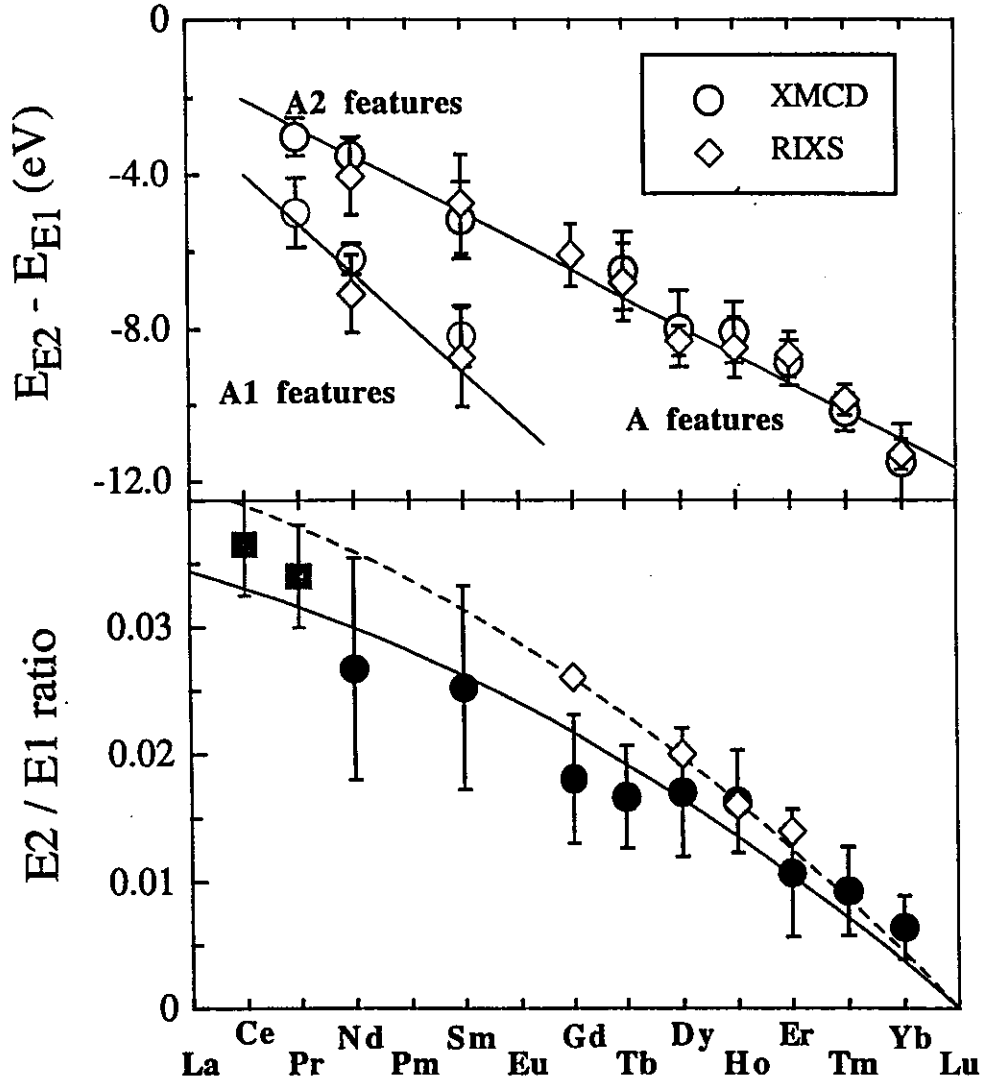

- Good agreement between features in the XMCD spectra and identified E1 and E2 absorption channels.
- Linear increase of E2-E1 excitation energy separation with increasing Z.
- E2/E1 intensity ratio follows expected functional dependence:~ $(14-n_{4f})(Z\alpha)^2$

Magnetic Circular Dichroism in X-ray Emission Spectroscopy

Difference in the x-ray emission for right and left circular polarized incident x-rays.

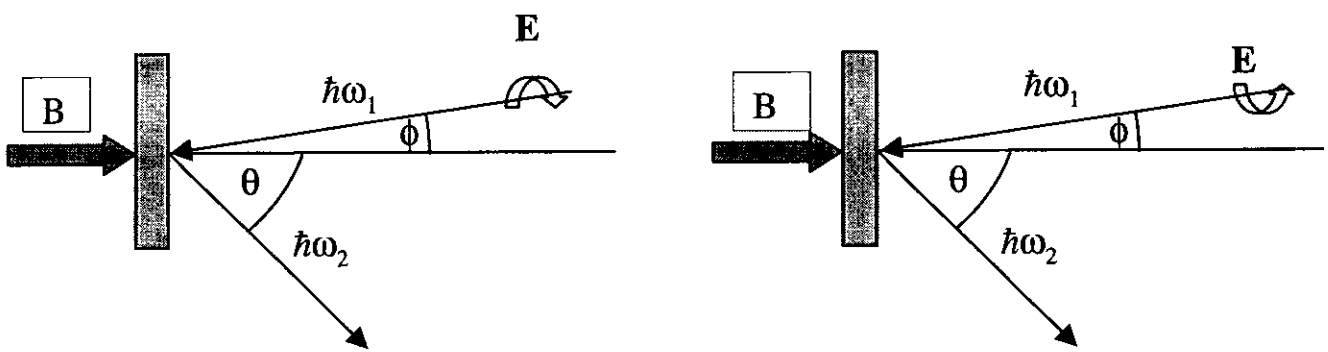

$$\Delta I^{MCD}(\varphi,\theta) = -\frac{1}{2}\cos\phi\left[\left(1+\cos^2\theta\right)\left(F_{+1,-1}+F_{-1,-1}-F_{+1,1}-F_{-1,1}\right)+2\sin^2\theta\left(F_{0,-1}-F_{0,1}\right)\right]$$

Magic angle: 54.7°

Magnetically aligned Gadolinium metal

- Beamline ID16
- HU52 helical undulator
- $\Delta E = 2.0$ eV

$L\alpha_1$: $3d^9 4f^7$ final state
$L\beta_{2,15}$: $4d^9 4f^7$ final state

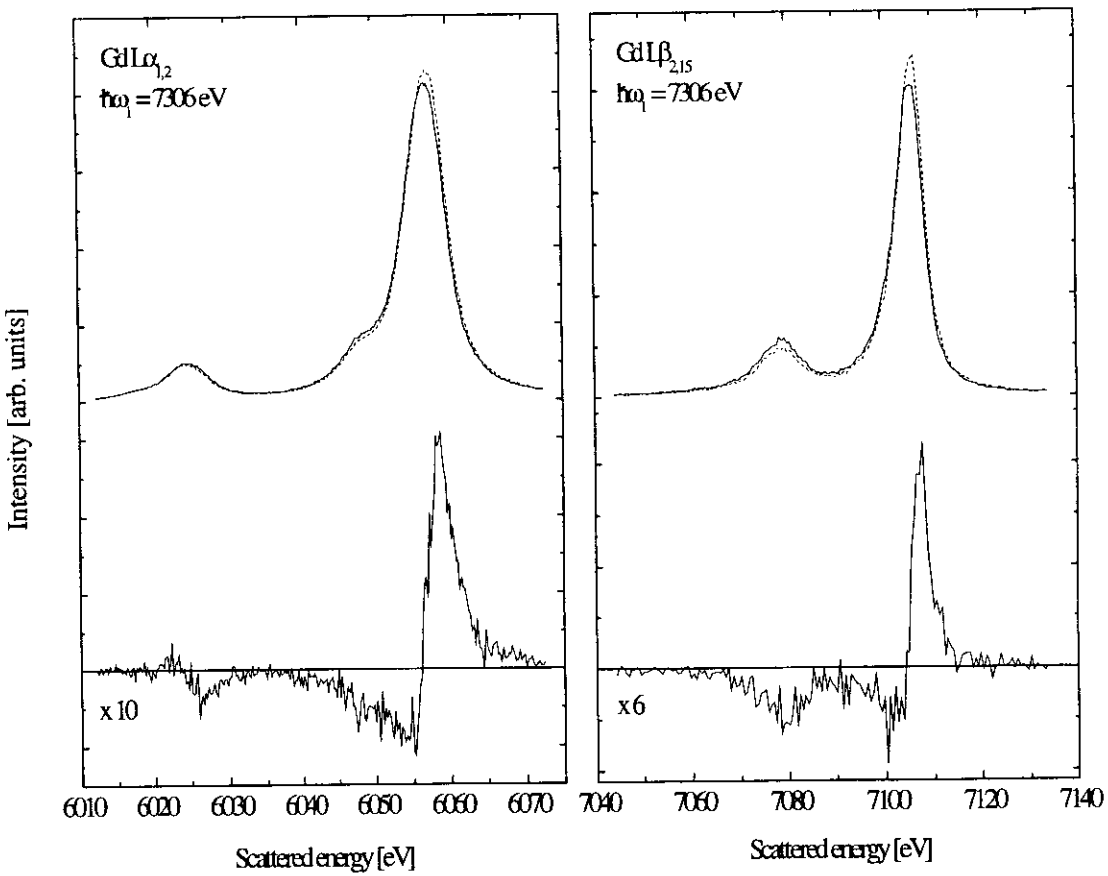

Excitation step: creation of a spin-polarized (deep) core hole ($2p^5$): $P_e = 0.25$

Emission step: polarized (shallow) core hole ($3d^9$, $4d^9$): ^2D
Polarized 4f-shell ($4f^7$): ^8S
Final state symmetry: $^{7,9}D$

Fluorescence line is composed of multiplet families with opposite magnetic character due to final state exchange interactions.

Simple one-electron picture

1. "spin-up" case, antiparallel spins, higher final state energy, lower $\hbar\omega_2$

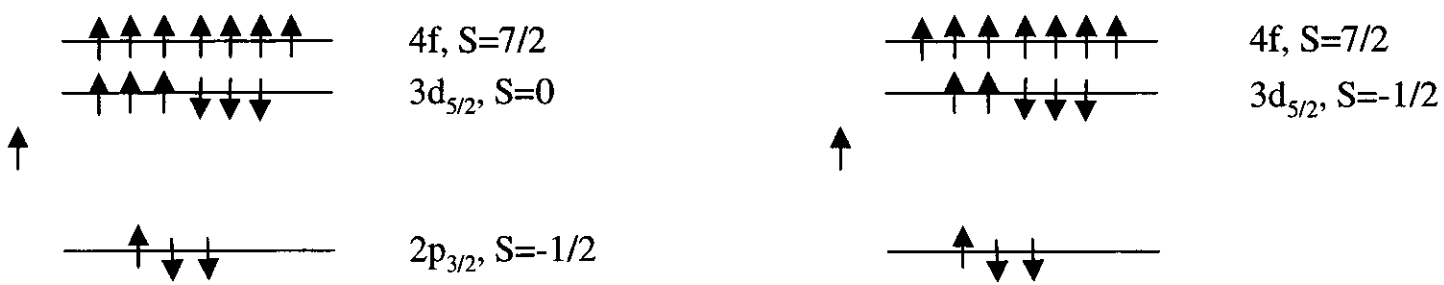

2. "spin-down" case, parallel spins, lower final state energy, higher $\hbar\omega_2$

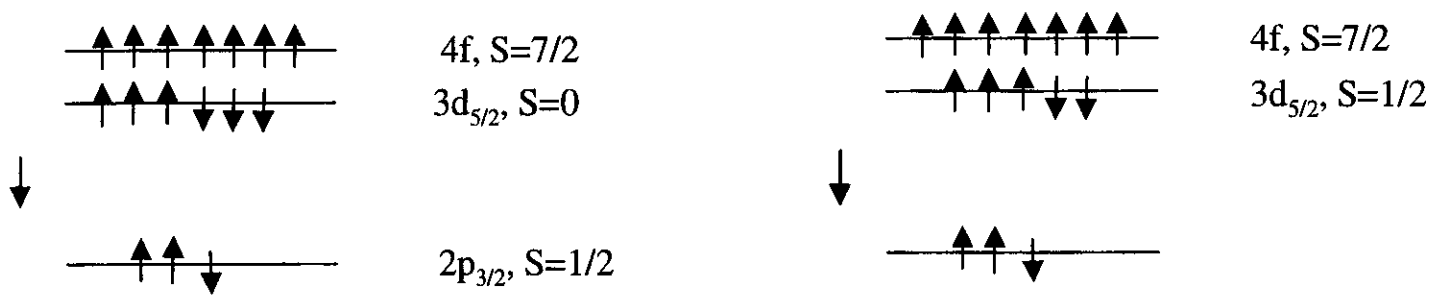

Atomic multiplet calculations

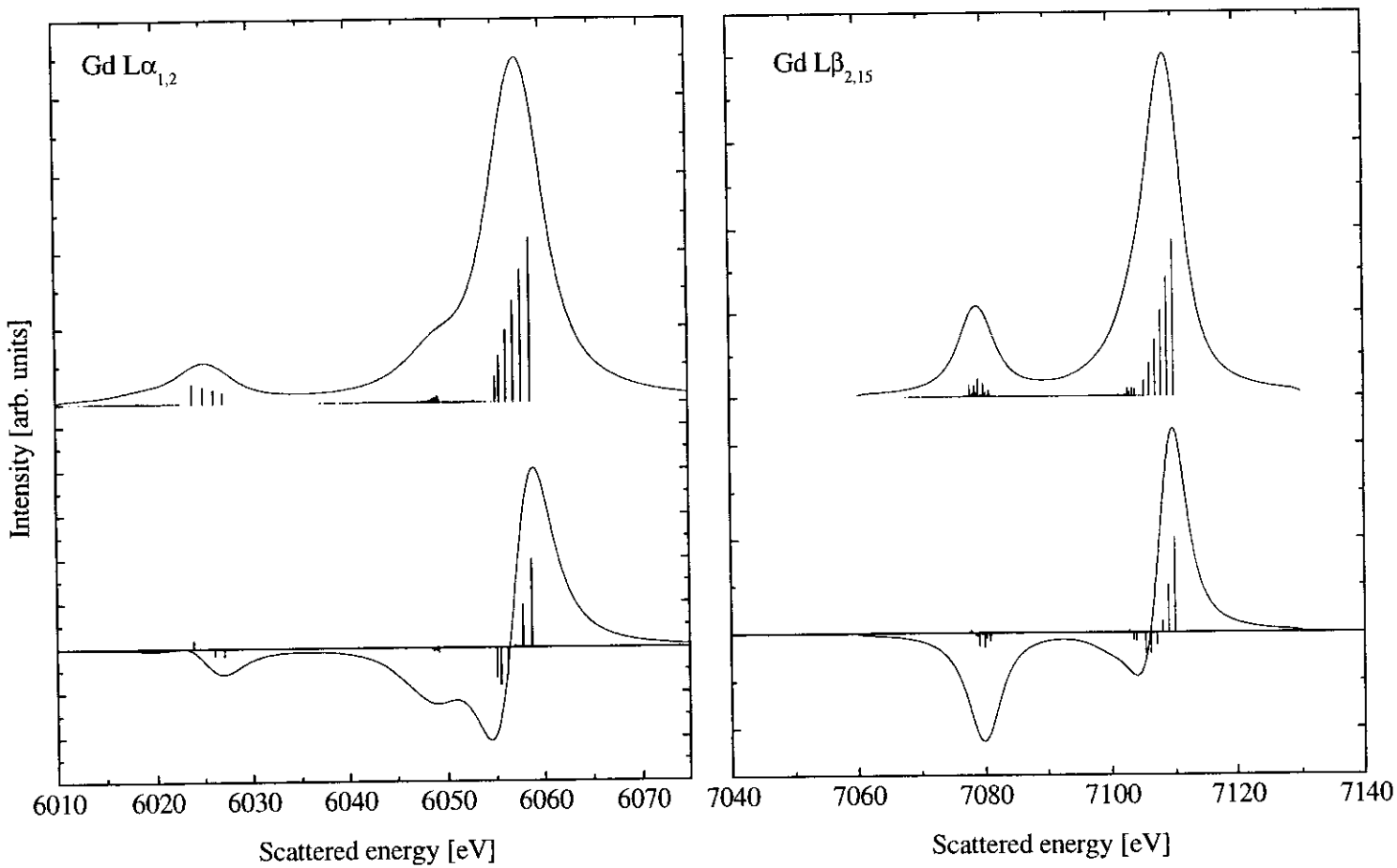

Lα emission:
spin-orbit coupling >> 3d4f exchange
(jj-coupling)

Lβ emission:
spin-orbit coupling < 4d4f exchange
(LS-coupling)

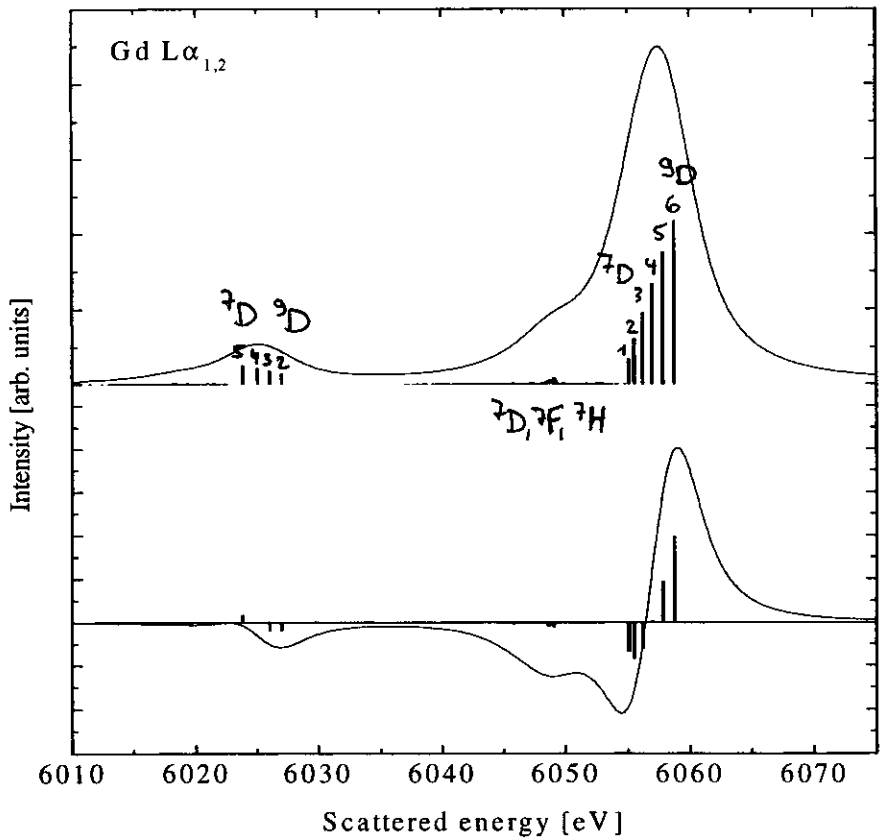

$j_{3d} = 5/2$

$^9D_6$ S(4f) ∥ S(3d) => lowest final state energy, $(\mathbf{L}\cdot\mathbf{S})_{3d} > 0$

⋮

$^7D_1$ S(4f) ∦ S(3d) => highest final state energy, $(\mathbf{L}\cdot\mathbf{S})_{3d} > 0$

$j_{3d} = 3/2$

$^9D_2$ S(4f) ∥ S(3d) => lowest final state energy, $(\mathbf{L}\cdot\mathbf{S})_{3d} < 0$

⋮

$^7D_5$ S(4f) ∦ S(3d) => highest final state energy, $(\mathbf{L}\cdot\mathbf{S})_{3d} < 0$

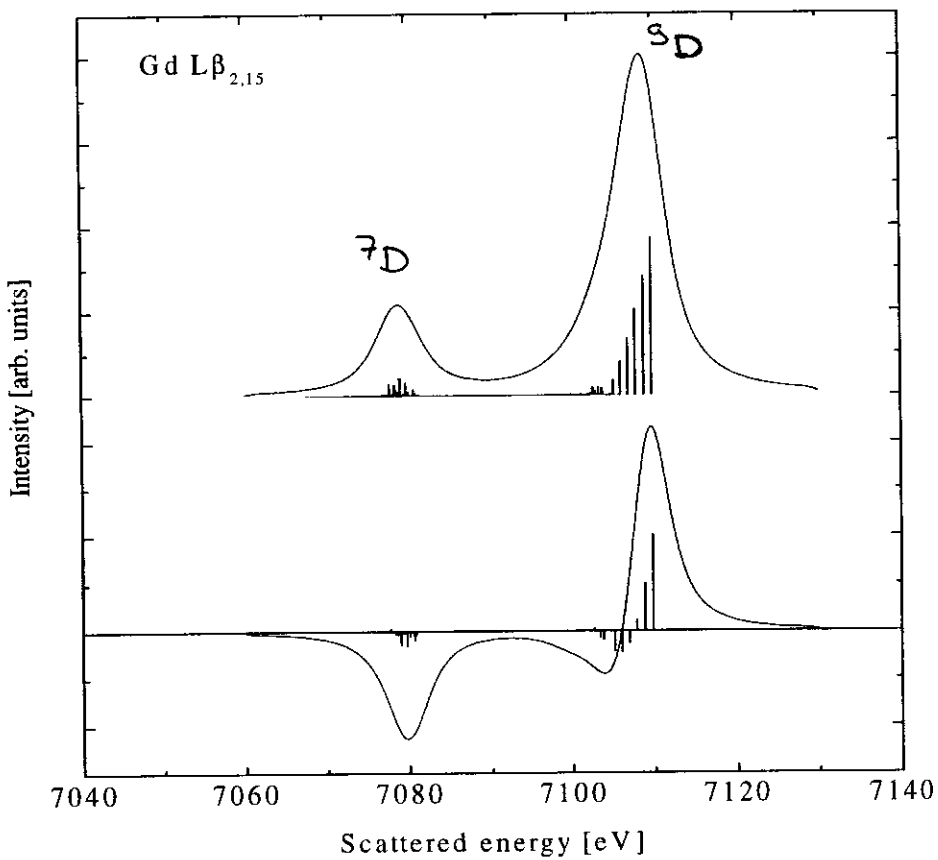

"High Spin"

$^9D_6$ S(4f) || S(4d) => lowest final state energy, $(\mathbf{L}\cdot\mathbf{S})_{4d} > 0$

⋮

$^9D_2$ S(4f) || S(4d) => highest final state energy, $(\mathbf{L}\cdot\mathbf{S})_{4d} < 0$

"low Spin"

$^7D_1$ S(4f) ∦ S(4d) => lowest final state energy, $(\mathbf{L}\cdot\mathbf{S})_{3d} > 0$

⋮

$^7D_5$ S(4f) ∦ S(4d) => highest final state energy, $(\mathbf{L}\cdot\mathbf{S})_{3d} < 0$

RIXS spectra recorded around L_3-absorption resonance

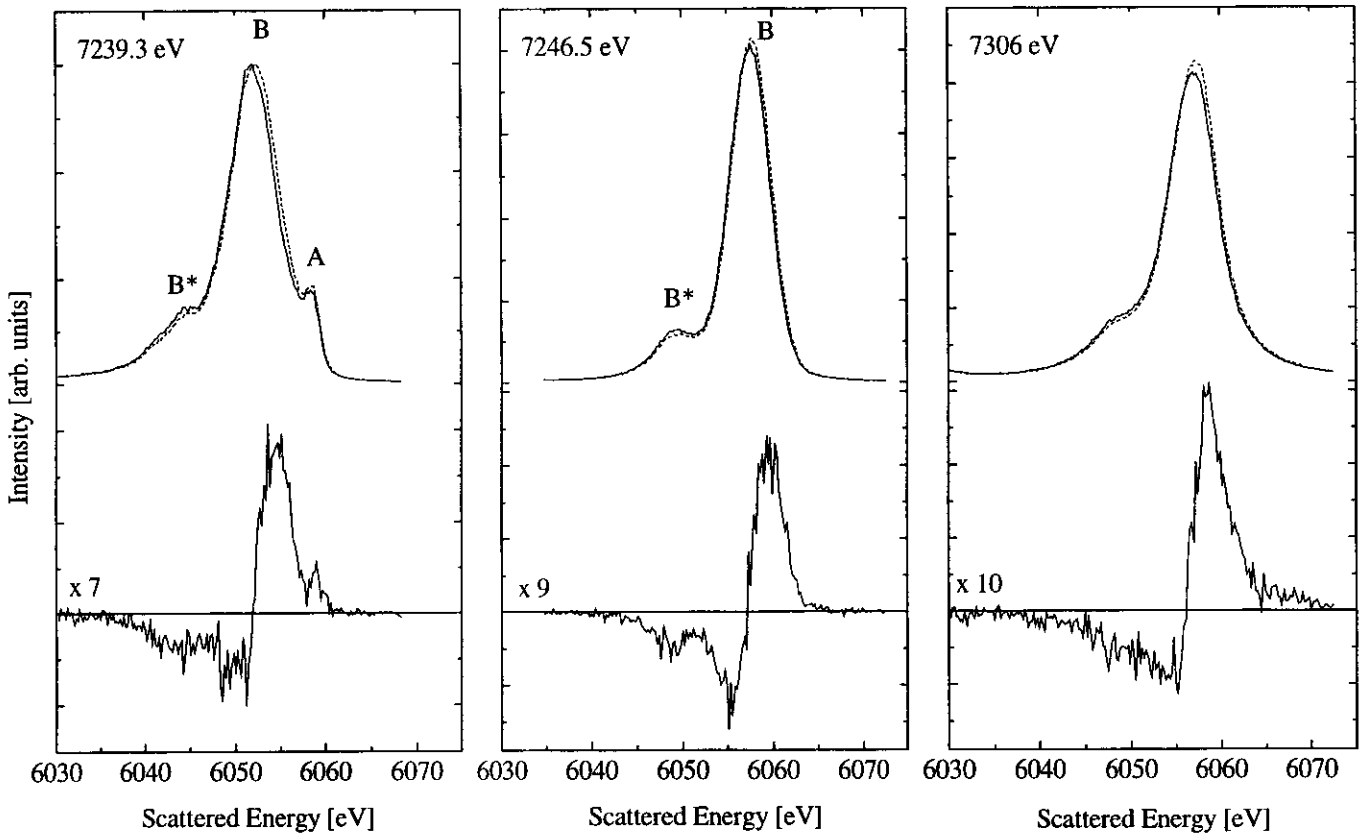

Pre-edge:	$3d^9 4f^7 5d^{n+1}$ (B,B') and $3d^9 4f^{n+1} 5d^1$ (A) final states
At white-line:	$3d^9 4f^7 5d^{n+1}$ (B,B') final states
Above edge:	$3d^9 4f^7 5d^1 e_k$ final states

Magnetic Linear Dichroism in X-ray Emission Spectroscopy

Angular dependence of the x-ray emission for linear polarized incident x-rays.

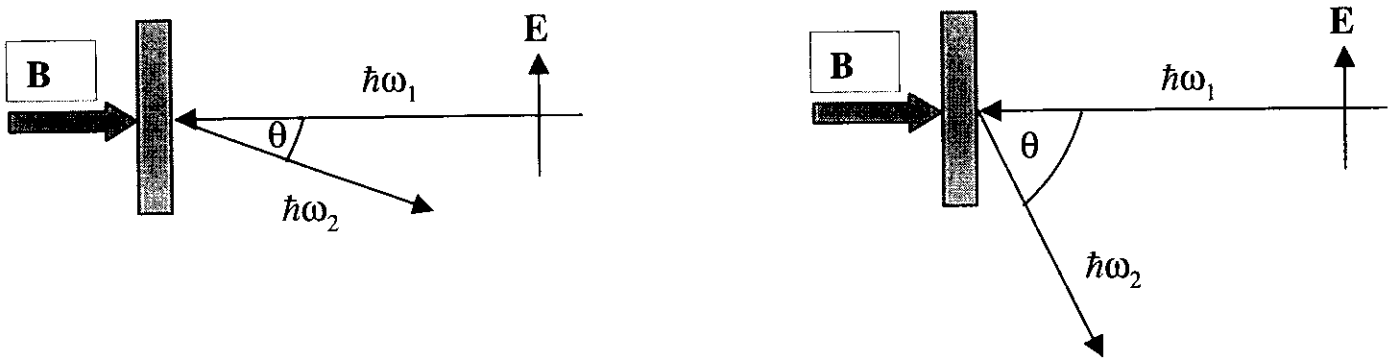

$$\Delta I_{LMD}(\theta) = \left[\left(1+\cos^2\theta_1\right)\left(F_{+1,q}+F_{-1,q}\right)+\left(2\sin^2\theta_1\right)F_{0,q}\right]- \left[\left(1+\cos^2\theta_2\right)\left(F_{+1,q}+F_{-1,q}\right)+\left(2\sin^2\theta_2\right)F_{0,q}\right]$$

For $\theta_1 = 0°$ and $\theta_2 = 90°$: $\Delta I_{MLD} = \left(F_{+1,q}+F_{-1,q}\right)-2F_{0,q}$

Yb 4d -> $2p_{1/2}$ x-ray emission in $Yb_3Fe_5O_{12}$

- Beamline ID16
- Excitation well above Yb L_2-threshold
- $\Delta E = 2.3$ eV
- θ=30° (dotted) and θ=70° (solid)

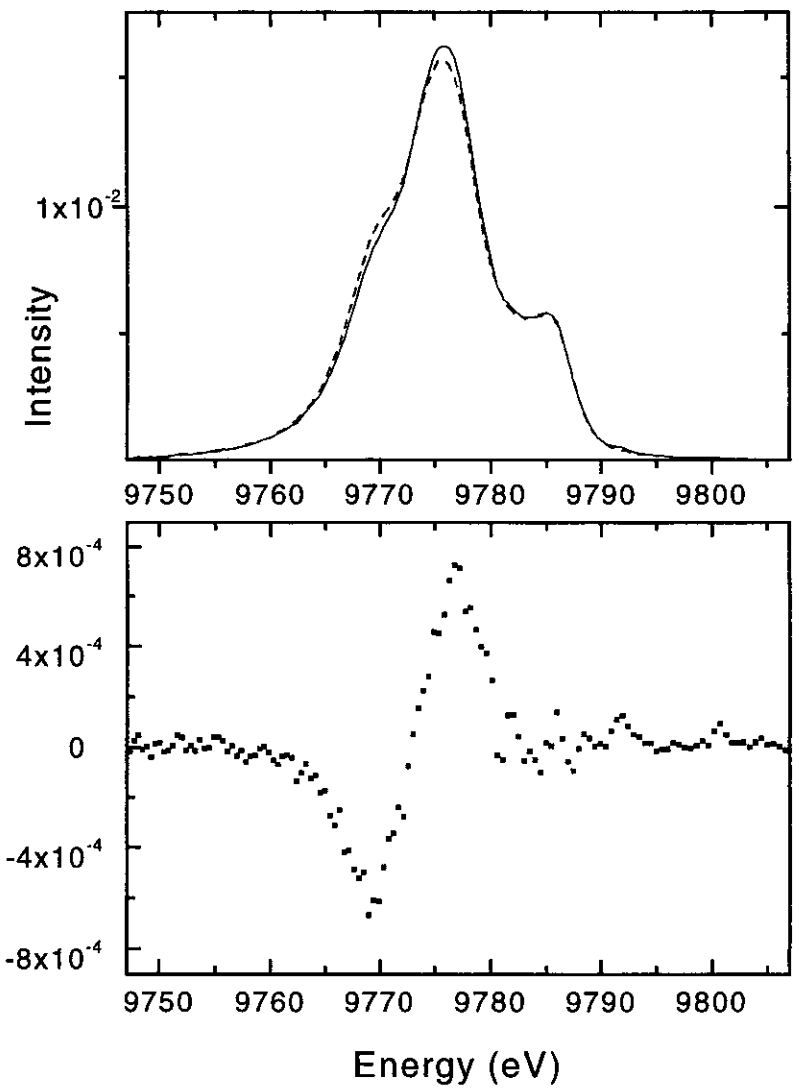

Comparison with atomic multiplet calculation

Reduction of the MLD effect due to:

- angular geometry (not θ=0° and 90°)
- incomplete magnetization of the Yb sublattice.

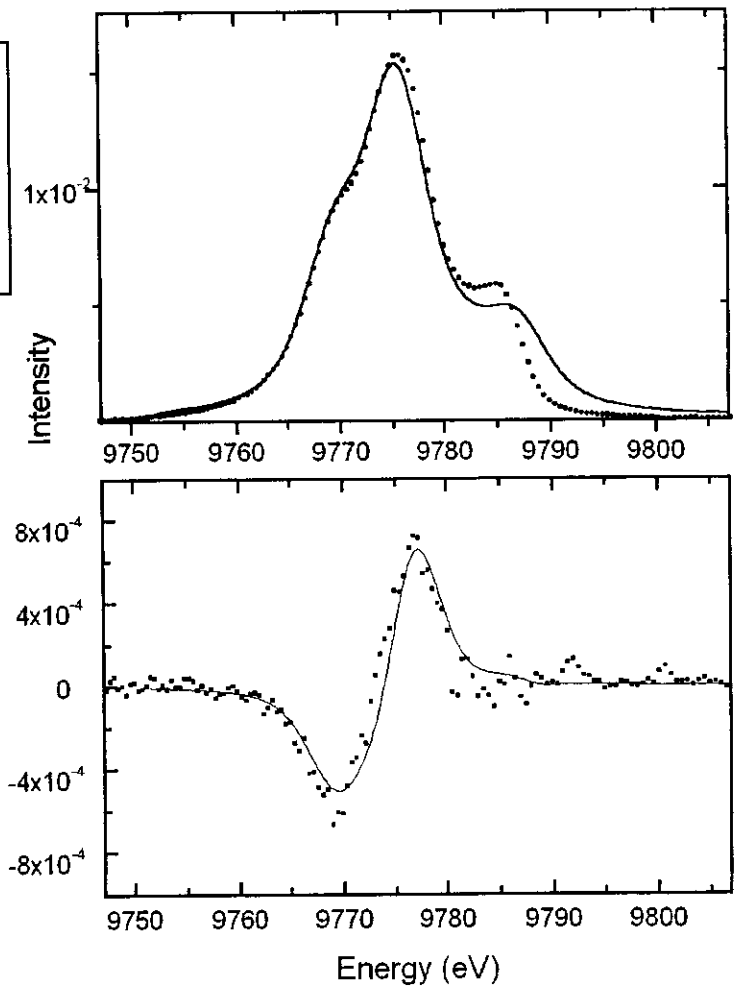

- Integrated intensity of LMD is zero.
- Amplitude is prop. to the Yb 4f moment.

Summary

MCD in XES: off -resonance:

- identification of character of the final state multiplet.
  (spin-orbit and exchange splitting, ...)
- amplitude of dichroic signal is prop. to magnetic moment.

at resonance:

- separation of dichroism arising from overlapping excitation channels.

LMD in XES: off-resonance:

- magnitude of dichroic signal is proportional to the 4f moment.
- hard x-ray probe for 4f moment.
  (no vacuum, bulk sensitive, access to buried layers, high pressure)

Magnetic Phase Transitions studied by Resonant Inelastic X-Ray Scattering

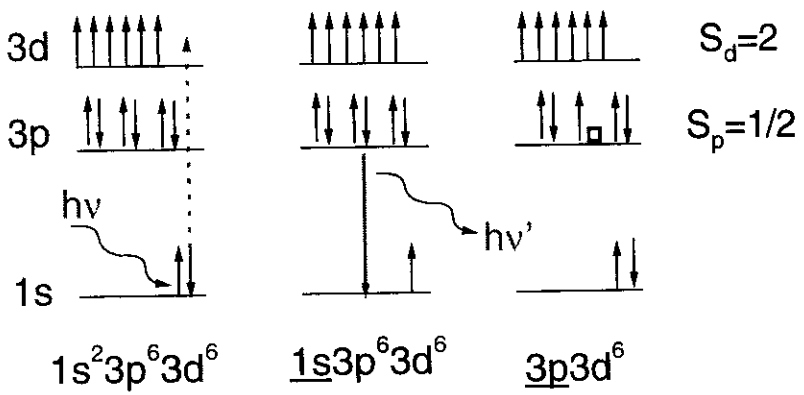

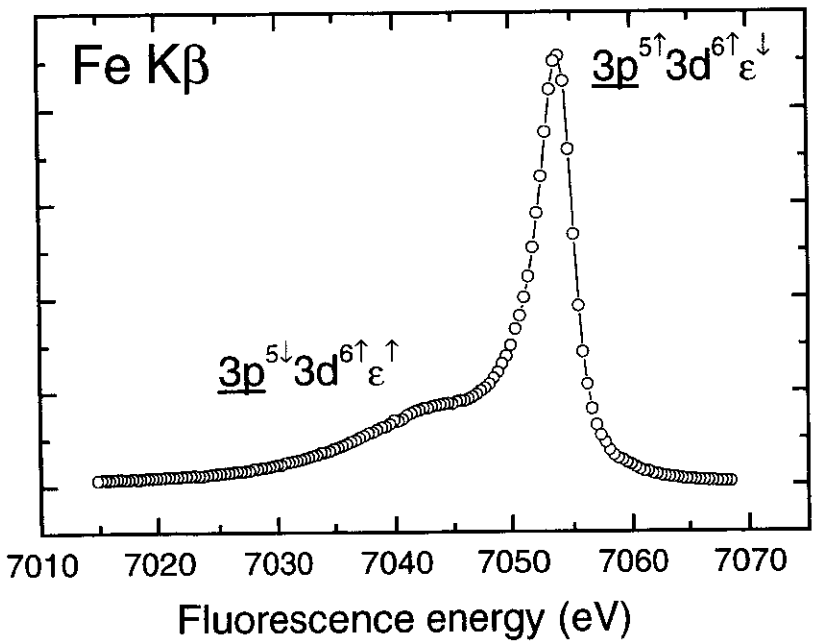

•Satellite structure arises from Coulomb- and exchange interactions between the 3p- and the 3d electrons.

- Main line: $S_d = 2$; $S_p = 1/2$, $e_{\downarrow}$ => spin-down character
- Satellite: $S_d=2$; $S_p= -1/2$, $e_{\uparrow}$ => spin-up character

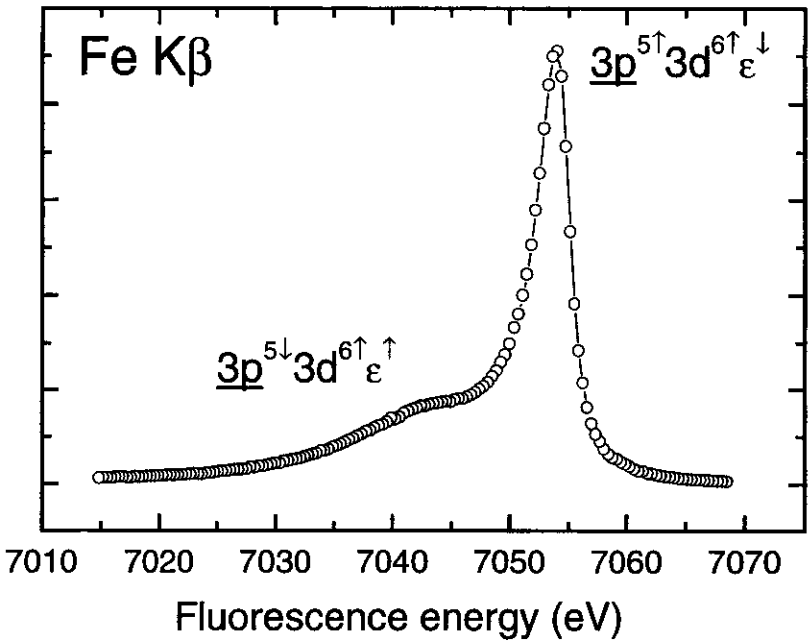

Evidence magnetic phase transition through changes in the emission line shape.

- intraatomic probe of the size of the 3d magnetic moment
- fast time scale: 10^{-15} s
- ferro-, antiferro-, ferri- and paramagnetic systems

Complementary to:

- X-ray magnetic circular dichroism (XMCD)
- Mössbauer spectroscopy

Pressure-induced ferromagnetic to non-magnetic transition in iron metal

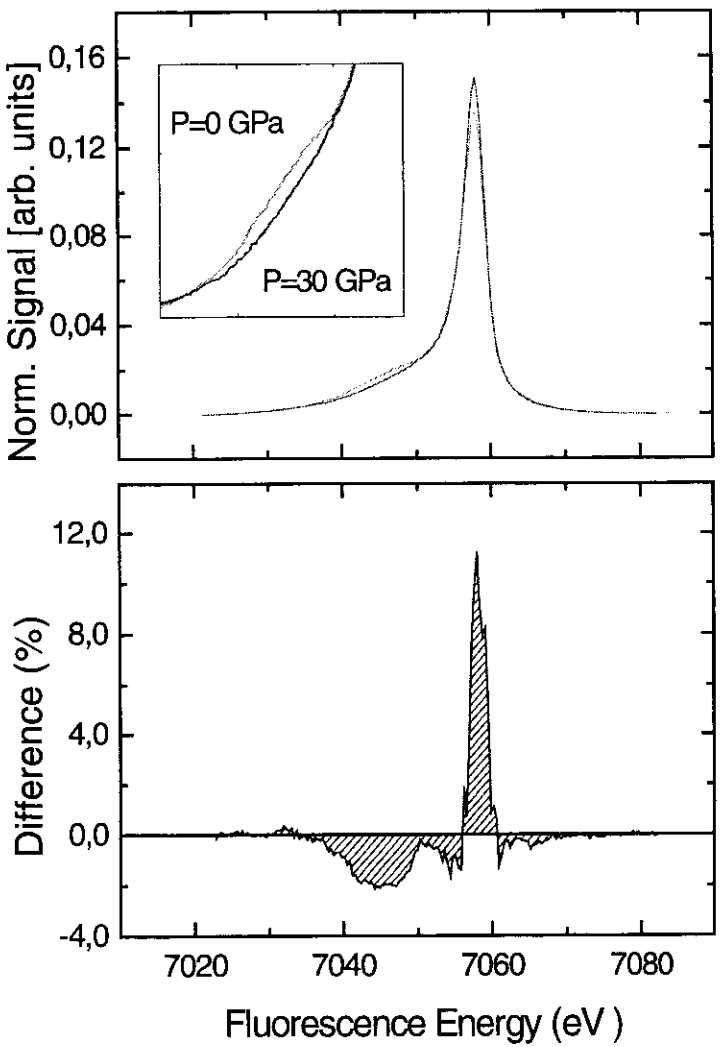

Simplified picture of the exchange split 3d- band

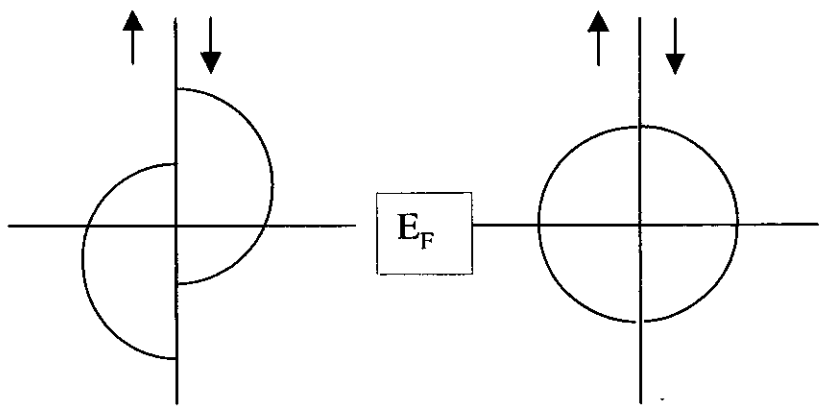

ferromagnetic non-magnetic

Ferromagnetic to non-magnetic transition in iron metal

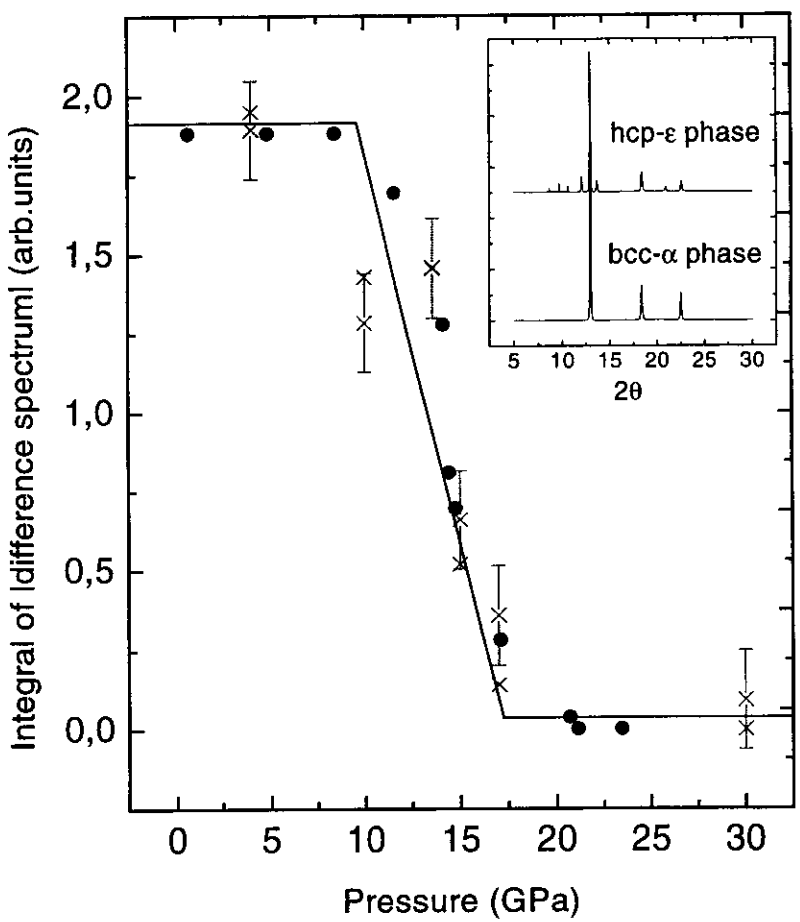

- Transition at about 13 GPa.
- Good agreement with Mössbauer and diffraction data.

X-ray emission from $Fe_{64}Ni_{36}$ Invar alloy

Invar characteristics: very small (invariant) thermal expansion over a large temperature range

First Interpretations: 2-γ state model (Weiss, 1963; Moruzzi, 1988)

- ground state high-spin / high volume
- excited state low-spin / low volume

• At finite temperature:
Thermal excitations to the LS state compensate for lattice expansion.

• At finite pressure:
decrease in volume induces transition to low-spin state.

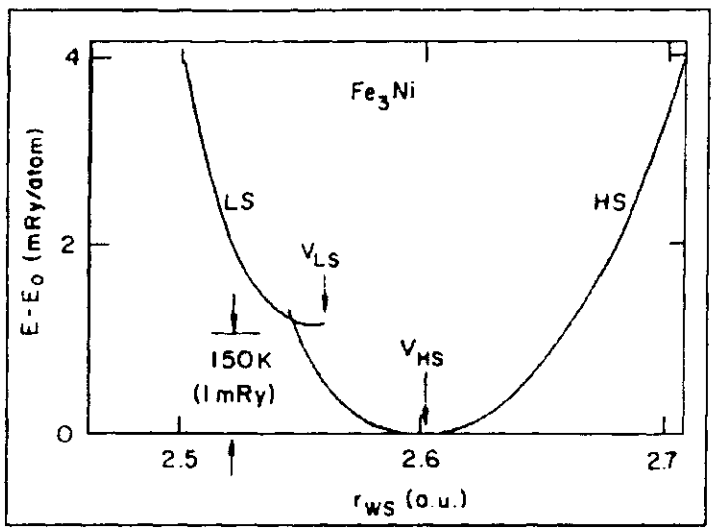

$Fe_{64}Ni_{36}$ pressure dependent measurements

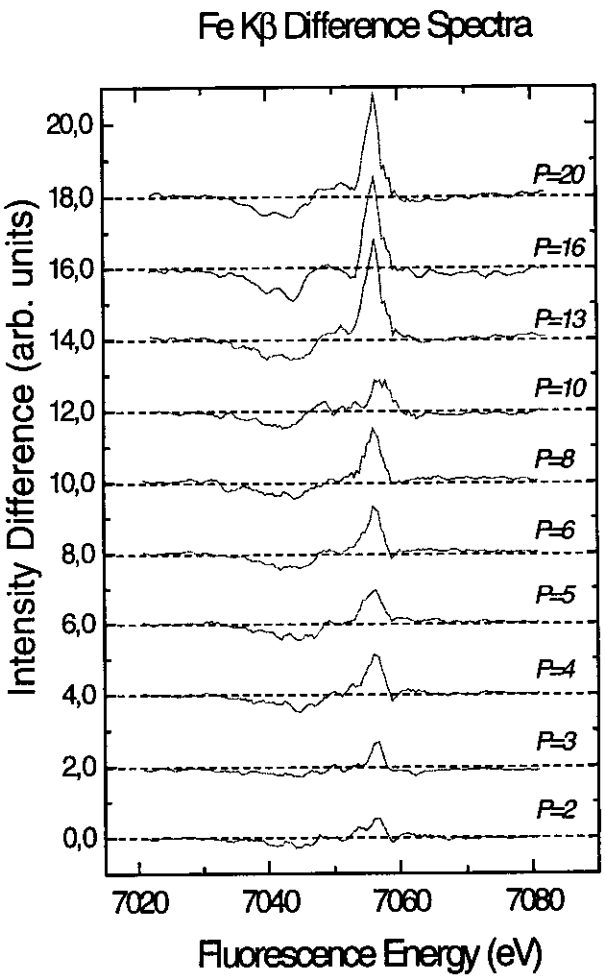

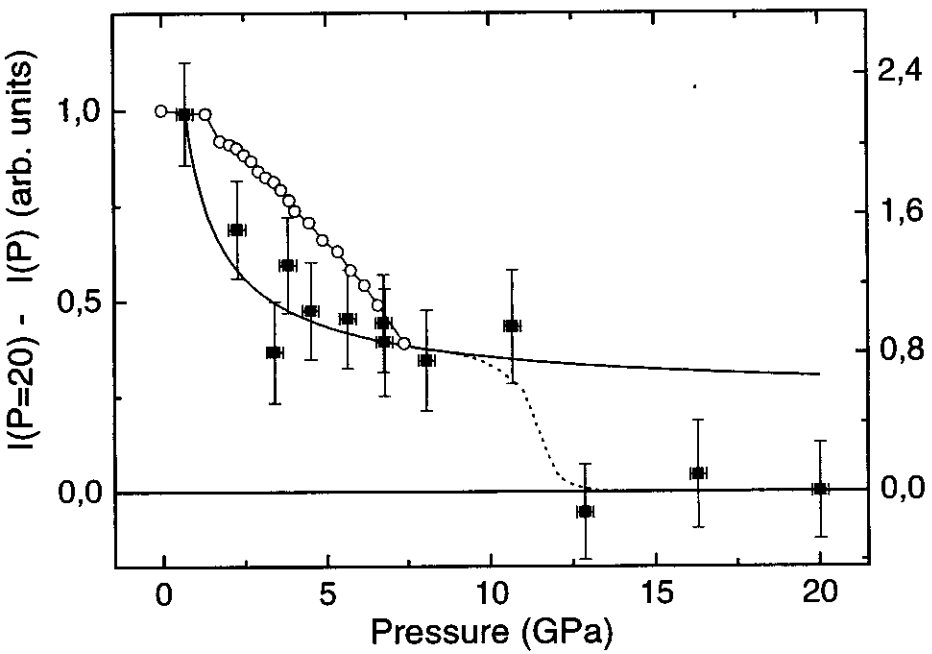

•Strong evidence of a two-step-mechanism:
HM -> LM -> NM

• For P < 5 GPa qualitative agreement with Mössbauer results.

•Same behaviour as observed in $Fe_{72}Pt_{28}$ Invar by Pt L-edge XMCD.

Summary

- Method is applicable to other TM compounds and the Rare-earth series.
  Vanadium to Cobalt (Nickel ?) ; Praeseodymium to Holmium
- Probe of the amplitude of the local 3d (4f) magnetic moment.
- Probe of local moment in ferro-, ferri-, antiferro- and paramagnetic systems.
- Method is complementary to XMCD and Mössbauer spectroscopy

- Polychromatic beam: Important enhancement of flux.
- monochromatic beam => exploitation of resonance phenomena.